Critical assessment of test cases on vortex breakdown over slender delta wing under static model conditions

Huang, Xing Zhong

RTO-TR-AVT-080 - Vortex Breakdown over Slender Delta Wings, pp. 2-1-2-40, 2009-10

Chapter 2 – CRITICAL ASSESSMENT OF TEST CASES ON VORTEX BREAKDOWN OVER SLENDER DELTA WINGS UNDER STATIC MODEL CONDITIONS

Xing Zhong Huang
Institute for Aerospace Research
National Research Council
1200 Montreal Rd.
Ottawa, Ont. Canada K1A 0R6

xingzhong.huang@nrc.ca

ABSTRACT

A critical assessment of more than thirty test cases on leading-edge vortex breakdown has been conducted. The test cases contain test data obtained on more than eighty wing configurations at high angles of attack and static model conditions. Special attention has been paid to related test conditions, such as model geometry, model blockage, model deformation under aerodynamic loads, wind tunnel wall and model support interference, the methodologies used in the experiments and the definition of vortex breakdown location. A screening process has been performed to help identify the relative merits of the various data sets and to extract reasonable confidence and quantitative information from the scattered database. This synthesized information is helpful to assess and validate numerical results.

List of Symbols

a	speed of sound in air
b	bevel width
c	wing chord
c_0	wing chord along the centre-line of the wing
h	height of a forward-facing step
M	Mach number, $M = \frac{V}{a}$
r	blockage, $r = \frac{S_{wing,\alpha=30}}{S_{test\ section}}$
Re_c	Reynolds number based on chord, $Re_c = \frac{V \cdot c}{\nu}$
Re_x	Reynolds number based on length, $Re_x = \frac{V \cdot x}{\nu}$
$S_{wing,\ a=30}$	wing projection area from front at α=30˚
V	velocity or flight speed
x	flat plate length in stream-wise direction

x_{VB} vortex breakdown location in ratio with wing centre-line chord, $x_{VB} = X_{VB}/c_0$

X_{VB} distance to vortex breakdown location measured along wing centre-line chord

α angle of attack

δ half bevel section angle

δ^* boundary layer displacement thickness

Δ_{max} difference between measured most downstream vortex breakdown location and mean vortex breakdown location

Δ_{min} difference between measured most upstream vortex breakdown location and mean vortex breakdown location

Λ angle of leading edge sweep

λ ratio of bevel dimension to boundary layer displacement thickness, $\lambda = \frac{b}{\delta^*}$

σ standard deviation

μ_0 viscosity of air

ν kinematic viscosity of air

ρ air density

2.1 INTRODUCTION

The tactical advantage of high maneuverability and agility has been the incentive for designers of fighter aircraft to continually expand the flight envelope of their designs. For such aircraft, slender or delta–type wings are often selected in order to gain extra aerodynamic force and control power while maintaining a compact structure over weight advantage. Modern combat aircraft routinely operate at high incidence and/or high angular rates, under which the flow field is usually dominated by strong leading-edge vortices, and where loss of controllability may be encountered.

In general, the flow over the delta wing surface may experience four different statuses of separation as the angle of attack increases. At low angle of attack there is no flow separation from the leading edge. The attached flow induces a leading-edge suction, which can be predicted from slender wing theory. As the angle of attack increases, depending on the leading-edge shape, flow separation starts to occur on the leading edge and progresses downstream as the second status of separation. A further increase of the angle of attack results in the third status: the formation of curved free shear layers and the vortex. The free shear layers roll up periodically into discrete vortical substructures. The substructures wind up spatially into a core over the leeward side of the wing forming a so-called leading-edge vortex. Further increasing the angle of attack leads to the last status: breakdown of the leading-edge vortex core. When breakdown occurs over a wing surface, it causes a sudden lift loss and a severe non-linearity in the aerodynamic loads.

Apart from non-linearity, vortex breakdown also causes a time dependence of aerodynamic loads. As a consequence, linear or local-linear aerodynamic models are no longer valid at flight conditions where vortex

breakdown occurs. Due to the lack of sufficient understanding of the flow physics and of reliable data sets, predictive capabilities have largely lagged behind operational requirements. A better insight into the vortex behavior, in particular vortex breakdown, is an essential requirement for developing CFD solutions and analytical models capable of adequately capturing the flow behavior in the advanced maneuvering regime.

For these reasons, for the past five decades, the behavior of leading-edge vortices, with special attention to vortex breakdown, has been the subject of a considerable number of experimental investigations as well as analytical and computational studies. On this subject, at least twenty theoretical and review articles were devoted.[1-20] However, due to difficulties inherent to vortical-flow experiments, measurements traditionally tended to produce qualitative rather than quantitative results. Furthermore, experimental results obtained on identical wings were seldom satisfactorily duplicated when tested in different facilities, with even relatively simple measurements of the vortex breakdown locations showing little correlation. Significant discrepancies are found in the data obtained by different investigators. Geometric variations, different test conditions, model deformations under aerodynamic loads, as well as differences in measuring techniques, significantly affected some measured results and contributed to the lack of correlation to the observations reported by others. A reliable assessment of the data generated in ground tests remains one of the most vexing problems to be solved in order to satisfactorily design military aerial vehicles and validate CFD codes. Thus, an evaluation of the existing experimental data sets was imperative so that the extensive work already performed at a very high cost could be properly used in the design of new military aerial vehicles and the development of analytical and computational models.

As vortex breakdown phenomena have important influences on aircraft performance, this paper attempts to extract as much useful and quantitative information as possible from critical examinations and correlations of existing data sets on vortex breakdown locations.

2.2 RESULTS ON MEASURED VORTEX BREAKDOWN LOCATIONS

A brief, but by no means complete, survey of published results for the time-averaged primary vortex breakdown locations over delta wings at static model conditions with leading edge sweep angles (Λ) ranging from 50º to 80º is depicted in Figs. 1 to 7. It is worthwhile to mention that most experimental results have not been corrected for wind/water tunnel wall and support interference effects and other test related effects. In order to facilitate further investigations, the model(s), test facilities and conditions of the referred test cases are listed separately in Table 1. As the 65° and 70° sweep delta wings are typical and closely related to high-performance military aerial vehicles, most attention has been paid to results reported for these two angles of sweep.

For $\Lambda = 65°$ and 70°, the preliminary comparisons shown in Figs. 4 and 5 reveal significant differences in the measured non-dimensional breakdown location, $x_{VB} = X_{VB}/c_0$, where X_{VB} is the distance from the apex to the measured vortex breakdown location and c_0 is the centerline chord. For $\Lambda = 65°$ and $\alpha = 22.5°$, for example, x_{VB} can be anywhere, from the trailing edge $x_{VB} = 1.0$ (Earnshaw[26, 27]) to $x_{VB} = 0.4$ (Lambourne & Bryer[24]). Similar scatter is found in the measurements on 70° delta wings. At $\alpha \approx 31°\sim32°$, the measured breakdown location varies from $x_{VB} \approx 0.8$ (Earnshaw & Lawford, et.al.[26, 27]) to $x_{VB} \approx 0.35$ (Wentz & Kohlmann[33-35]). Finally, for $\Lambda = 70°$,and $\alpha \approx 31°\sim32°$, one data set (Wentz & Kohlmann[33-35]) exhibits a “knee’, reflecting a rapid, possibly discontinuous movement of the breakdown location from mid-chord to aft of the trailing edge over a small change in the angle of attack. The large scatter in the measured vortex breakdown locations and

the possible presence of the discontinuity leads to different understanding and explanations[101,109,112]. This uncertainty will also jeopardize any attempt to model the vortex breakdown behavior.

Given that the vortex breakdown is basically an unsteady, non-linear and time dependent process, some uncertainty in the measurements of the breakdown location is to be expected. Furthermore, the effects of the proximity of wind tunnel walls and support geometry, model blockage and model deformations under the aerodynamic loads increase the scatter in the measurements. These effects unavoidably degrade the consistency of results. In addition, the experimental data given in the reports also depend on the criteria and the methodology used to define the breakdown location, e.g. whether a laser sheet is orientated normal to or along the vortex axis, seeding injection method, Schlieren system set-up and experimental accuracy. All of these considerations complicate the assessment.

On the other hand, it has been found that in a given investigation, the breakdown location can be very stable with high repeatability if the test conditions are well maintained [92, 112, 126]. As examples, Fig. 8 depicts the standard deviations, σ, as well as maximum and minimum deviations, Δ_{max}, Δ_{min}, of the breakdown location for a 75° delta wing[112] at $Re_c = 1.5x10^4$, while Fig. 9 shows Mitchell's[126] results conducted at $Re_c = 1.56x10^6$ for a 70° delta wing. Those figures clearly show that the deviation of breakdown location is small, although a slightly increased scatter in the data can be observed when the breakdown location occurs over the aft part of the model. Lowson & Riley[90] repeated the experiments of Wentz & Kohlman[33] and Lambourne & Buyer[24] and found Wentz & Kohlman's data to be repeatable if the models and test conditions were accurately reproduced.

2.3 CRITERIA OF THE ASSESSMENT

In the author's opinion, the fundamental issue for assessing the data sets is not which data sets are "good" or "bad" but what kind of data sets are necessary, suitable or representative to certain flow conditions. The assessment in this paper is mainly a filtering process for screening the available data. In principle, the sources of discrepancies for the same normalized model geometry in different experiments could result from facility-related or simulation-related sources. The former include free-stream conditions (such as flow non-uniformity, angularity, unsteadiness and noise), wall and support interference and test condition repeatability. The later include Reynolds number based on c_0, Mach number and differences in detail model dimensions, i.e., the shapes of leading edges, trailing edges, fairings and centre-bodies. Those sources will be investigated as much as possible so that the process will lead to a better reconciliation of the different results. The assessment consists of the following main steps:

a) Collect as many data as possible relating to vortex breakdown. Pay more attention to the described test conditions.

b) Weigh the accuracy of those data in terms of the quantitative or qualitative information about the test conditions.

c) Normalize the various data sets into "equivalent" delta wings having sharp leading edges and a flat upper surface by relying on the well accepted assumption that for a delta wing with a flat upper surface and sharp leading-edges, x_{VB} is independent of Reynolds number. Correct for Reynolds number effects on other leading-edge shapes such as leeward bevels and rounded edges.

d) For the data sets with many parameters, preference is given to the data sets where a minimum number of other parameters is varied.

e) As different experiments employed different leading-edge shapes and centerbody settings, clarification of these effects is the prerequisite for the assessment.

2.4 EFFECTS OF LEADING-EDGE SHAPE, CENTERBODY AND DIFFERENT TEST CONDITIONS

2.4.1 Leading-Edge Shape Effect

Since boundary layer separation initiates from the leading-edge (where the vorticity flux inside the boundary layer is transported to the free shear layer and eventually rolls up into a vortex) then leading-edge shape may affect the vorticity flux and the effects of leading-edge geometry have to be considered.

Basically there are two kinds of leading-edge: sharp and round. A leading edge is defined as "sharp" if the boundary layer separation line coincides with the junction line of the upper and the lower wing surfaces and if the separation onset is fixed and at the apex of the wing. A leading edge is defined as "round" if, the separation line is not fixed and the onset of the separation is also not from the apex. Furthermore, with a round leading edge, both the separation line and the separation onset will move depending on the flow conditions.

Kegelman & Roos[60], Pelletier[91,93], Huang[112,136,140], Luckring[100-103,132,135,139], Wentz and Kohlmann[34] conducted experiments while Pirzadeh[141] applied CFD methods to investigate the effect of leading-edge shape on vortex behavior or vortex breakdown.

For a sharp leading-edge, the effect of leading-edge bevel may lead to changes in effective angle of attack. If the bevel size is large enough, as a first approximation, the following equation for modifying the effective angle, $\Delta\alpha$, at static model conditions and at high Reynolds number, may apply[76, 82, 87].

$$\Delta\alpha = \tan\Lambda * \cos\delta \qquad (1)$$

However this equation can only be used conditionally. For example, the results of Kegelman and Roos[60] show that the change in effective angle of attack is only 1/3 of the value predicted by the above equation. In contrast, the water tunnel experiments of Pelletier[91,93] and Huang[114] exhibit negligible difference in x_{VB} between different leading-edge shapes. Likewise, Wentz & Kohlmann's [34] results of breakdown location for a 60° delta wing with either beveled or square leading edges are very similar. On the other hand, the studies of Hanff and Huang[104] and Huang, Mebarki and Benmeddour[140] at high Reynolds numbers with large leading-edge bevels show that the breakdown locations are almost 20% farther downstream than others' on models with small size leading-edge bevels. This change is equivalent to a decrease of 4º in effective angle of attack. Similar information can be found from airloads and pressure measurements. Huang[136] and Huang et al.[140] reported that the measured normal force exhibits two discontinuities: one corresponding to vortex breakdown near the trailing edge and one corresponding to breakdown at the apex. These references show that for a delta wing with a bevelled leading-edge, the latter discontinuity appears on the angle of attack 4º higher than that with a flat upper surface (Fig. 10a and Fig. 10b) indicating the effective angle of attack on the bevelled wing model may be 4º less than that with the flat upper surface wing model.

From the above discussion it follows that equation (1) cannot be applied in isolation without considering other additional factors. One important fact appears to be the ratio, λ, of the size of the bevel (e.g. bevel width, b) to the thickness of the boundary layer in the vicinity of separation, δ^*. Thus,

$$\lambda = \frac{b}{\delta^*}$$

The breakdown location, x_{VB}, varies directly with λ. It can be imagined that if $\lambda << 1$, the bevel acts as local or minor disturbance while the large flat upper surface, which is downstream of the bevel, will be the geometric feature that has a global effect on the flow. Actually, in the experiments of Wentz & Kohlmann[111] and Pelletier[91,93], λ was 1/15 and 1/7 of that in the experiments of Hanff & Huang[104], explaining the negligible bevel effect in the former as compared to that in the latter. The water tunnel experimental results reported by Huang[114] with $\lambda > 1$ also confirm that if the bevel on the leeward side is large enough it will delay the vortex breakdown. The reduction in angle of attack is close to the value estimated from equation (1).

In order to quantitatively analyse the effect of relative size of the leading-edge bevel, λ, on the flow, it is worthwhile to look at typical permissible surface discontinuities that may have negligible effect on boundary layer flow. Braslow et al.[61] found the allowable forward-facing step height, h, for a flat-plate in a laminar boundary-layer and a zero pressure gradient is roughly:

$h(\text{ft}) \approx \frac{1800}{\text{R}/\text{ft}}$, where Re_x/ft is the Reynolds number per foot.

For a Reynolds number of $\text{Re}_x = 1\text{x}10^6$/ft, the typical permissible surface discontinuity is roughly h = 0.025in, while the boundary layer displacement thickness, δ^*, on a 2-D flat plate can be determined from Blasius profile[141]:

$$\delta^* = 1.72\sqrt{\frac{\nu x}{u_0}}$$

where u_0 is the velocity in the free stream, x is the length of the plate and ν is the kinematic viscosity.

At this Reynolds number (i.e. $\text{Re}_x = 1\text{x}10^6$/ft) and the chordwise location (x), δ^*, is estimated to be 0.06in. From the two numbers, h and δ^*, in the example, it can be concluded that if λ is approximately less than 0.4, the disturbance caused by the surface discontinuity may be neglected.

For a round leading-edge, if the relative bevel size, λ, is relatively small, the above analysis may still be valid and the effect of the rounded leading-edge shape could be ignored. However for relatively large size of rounded leading-edge, the experiments of Huang[136], which examined the normal force, show similar results between wings with bevelled and rounded leading-edges, indicating the difference of time-averaged vortex breakdown locations between those wings might be small. However, it does not mean that the vortex behavior is similar. Luckring[132,135,139] and Huang et al.[140] conducted experiments respectively to investigate the leading-edge shape effect on the flow behavior at high Reynolds numbers. Luckring applied very dense pressure orifices while Huang et al. applied PSP technology as well as pressure orifices to study the pressure distribution and related airloads. Huang et al.[140] also digitized the PSP images to obtain the pressure distribution along different lines, either at different chordwise locations or at different conical lines starting from the apex. As examples Luckring's results for the comparisons between a sharp and round leading-edge delta wing at M=0.4, $\text{Re}=6\text{x}10^6$ and $\alpha=10^o$ are shown in Fig. 11, while Huang et al.'s PSP images, digitized pressure distributions along different lines on the PSP images are illustrated in Fig. 12 to Fig. 14. Luckring's and Huang et al.'s results at different chordwise locations clearly show that for a rounded leading-edge the attached flow pressures are apparent in the forward potion, while leading-edge vortex-like pressures appear

in the rear potion. The separation onset or the origin of the leading-edge vortex on a rounded leading-edge is not at the apex but somewhere downstream of the apex. The PSP images in Fig. 12a exhibit that for sharp leading-edge the high suction area (blue area) is conical and originates from the apex, while for a rounded leading-edge the suction area is not conical (Fig. 12b). The enlarged PSP images in the forward part (Fig. 12c) show that the blue line in the forward part is very close to the edge, indicating the attached flow induced leading-edge suction in that area. The digitized spanwise pressure distributions clearly show the attached flow induced suction along the round leading-edge (Fig. 13). The digitized pressures along a conical line on a sharp leading-edge or along a line (shown in the figure) are shown in Fig. 14. It appears that the suction peak is further upstream and stronger on a round leading-edge than that on sharp and beveled leading-edge.

Pirzadeh[142] applied Navier-Stokes solutions on three leading-edge cases. His results show quite different flow behavior between sharp and rounded leading-edges. As examples, Fig. 15a to Fig. 15c show the velocity vectors on cross-sectional planes at the mid-root-chord station. These Figures clearly show that the size as well as the height of the primary vortex decreases as the radius of the leading-edge increases. Although as he pointed out that the accuracy of vortex flow computations, especially those featuring vortex breakdowns, is highly susceptible to the local grid resolution, and vortex flows induced by blunt leading-edge present an even greater challenge to CFD, such as turbulence models, flow transition, and other numerical elements that influence the accuracy of predicted flow separation, nevertheless the comparison is physically acceptable.

From the above analysis, the following conclusion may be drawn:

a) The leading-edge shape may not cause a significant effect on vortex breakdown location if the size of the different shapes is relatively small.

b) If the size of leading-edge shape is relative large compared to the thinness of the boundary layer, the effect of leading-edge shape on the vortex can not be ignored and the amount of the effect depends on the shape of the leading-edge.

c) For large size, sharp and beveled leading-edges equation (1) may be used to approximately modify the effective angle of attack and corresponding vortex breakdown location.

d) For large size but rounded leading-edge, there appears attached flow in the forward part and the attached flow induced suction is very close to the edge area. The separation line and its onset are not fixed and are dependent on the test conditions. The corresponding vortex breakdown location, in general, will be downstream of that obtained with a flat upper surface but close to that with a beveled and sharp leading-edge.

2.4.2 Centerbody Effects

In many experiments, a centerbody was inevitably required to house the balance and/or the model's support. Also a centerbody is commonly used in unmanned combat aerial vehicle (UCAV). Since a centerbody is different from a forebody, investigation of centerbody effects is not only of interest in assessing the experimental data but it can also be useful in the design of the new UCAV and similar aerial vehicles. A centerbody is usually located aft of the leading-edge and in the separation zone. As a result, its effect is even more difficult to analyse than that of forebody.

Pelletier[91, 93], Huang[114], and Huang et al.[140] investigated centerbody effects in wind tunnel or in water tunnel experiments by comparing the results with and without centerbody in the experiments. Huang's results

conducted in a water tunnel at a Reynolds number $Re_c \approx 1.5x10^4$ shows that the centerbody effect on vortex breakdown location is negligible except when the vortex breakdown location is near the trailing edge. This may be caused by the sudden expansion of the flow at the end of the centerbody. Similar trends can be found in the experiments of Pelletier[91,93] and Huang[140] where the Reynolds numbers are $1.5x10^5$ and $2.4x10^6$ respectively. The PSP and pressure orifice experiments of Huang[140] conducted at higher Reynolds numbers ($Re_c \approx 2.4x10^6$) are shown from Fig. 16 to Fig. 17. Huang's pressure orifice measurements at different chordwise locations with and without a centerbody show that the centerbody only causes a local effect and no global effect is observed. Other than those experimental results, Benmeddour, Mebarki and Huang[148] conducted numerical studies with and without centerbody[148]. They applied the in-house solver, FJ3SOLV, and the commercial software, CFD-FASTRAN, to calculate the effect of the centerbody on the surface pressure over a 65° delta wing and a 55° diamond wing. Their CFD results are shown in Fig. 18 to Fig.21. In general, their CFD results agree with experimental results. It may be concluded that a centerbody, with the size and shape as in the these studies, has negligible global effects on the aerodynamic characteristics.

2.4.3 Reynolds Number and Mach Number Effects

It is well accepted that with a sharp leading-edge the vortex breakdown location is approximately independent of Reynolds number. The time averaged pressure distribution is also less affected by the Reynolds number as shown by Luckring[139] (Fig. 22). However, the amount of unsteadiness in the vortex depends on the Reynolds number. This unsteadiness may cause oscillations in vortex core location, vortex breakdown location and interactions between the left and right vortices. Thus, the measured time-averaged locations of vortex core and vortex breakdown may be nearly the same, but the time-dependent value and the asymmetry of the two vortices will depend on the Reynolds number, thereby resulting in increased scatter in the measurements and even bifurcation when tested at higher Reynolds number.

The Reynolds number related unsteadiness in the vortex comes from many sources. First, depending on the Reynolds number, the vorticity within the boundary layer may transport discontinuously into the free shear layer. Second, the Reynolds number will affect the type of Kelvin-Helmholtz (K-H) instability. At high Reynolds number, discrete and small-scale vortices appear and follow a helical trajectory around the core resulting in another source of unsteadiness. Thirdly, when a vortex breaks down at high angle of attack, at high Reynolds number there is ample unsteadiness within the breakdown region. This gives the flow in the vicinity of the spiral a spatial and temporal periodicity. Finally, at high Reynolds number, there exists a strong axial and related spiral fluctuation in the vortex breakdown location. The time history of breakdown location consists of low-frequency, large-amplitude fluctuations and high-frequency, low-amplitude fluctuations. As examples Huang[144] presents pressure spectral measurements conducted at high Reynolds number which show that there is a peak at low frequency when vortex breakdown moves over the wing area (Fig. 23).

The above facts show that the Reynolds number effect may not cause too much effect on time-averaged vortex breakdown location over a delta wing with a sharp leading-edge, but the time-dependent behavior will be much affected by the Reynolds number.

In order to understand Reynolds number effects on the unsteadiness of the vortex, the unsteadiness at different Reynolds numbers has been the focus of extensive research. Some examples are shown below. Results from experimental and computational studies regarding the effect of Reynolds number on the free shear layer are shown in Fig. 24 and Fig. 25 to Fig. 26 by Lowson[58, 117] and Visbal[92, 97] respectively. They found that at low Reynolds number the free shear layer is laminar. As Reynolds number increases, the free shear layer transitions from laminar to turbulent at somewhere along the leading-edge. Visbal further found

that the transition progresses toward the apex as Reynolds number increases further (Fig. 25 and Fig. 26). The instantaneous azimuthal vorticity distribution in a plane passing through the vortex axis obtained by Rockwell [88] is show in Fig. 27. Gursul[95] measured time histories of breakdown locations which are illustrated in Fig. 28. Huang used high speed visualization method to study the unsteadiness inside the vortex breakdown at high Reynolds number ($Re_{c0}=3.6x10^6$). Following Lambourne's[29] description of vortex breakdown, in Fig. 29 Huang[112,142] denoted the vortex filament kink point as "point A" while the vortex breaks down into large scale turbulence as "point B". Huang found that the unsteady behaviors of points A and B are quite different. As examples sequence of frames of the images are shown in Fig. 29. In the sequence, point A moves in excess of $0.1c_0$ while point B remains more or less stationary. The speed of response of point A corresponds to half convection speed, i.e. $0.5V_\infty\cos\alpha$, whereas point B barely moves at all. Thus if the kink point is defined as the vortex breakdown location as in most of researchers' measurement, the fluctuation of point A will deteriorate the measurements. On the other hand, if the point B is taken as the vortex breakdown location as Huang and Hanff[82] did in a section view of laser-smoke sheet normal to the vortex axes, the breakdown location will be 0.1 c_0 downstream of the point A which is defined as breakdown location by others' experiments.

For a round leading-edge, the Reynolds number effect is more complex. As mentioned above there is attached flow in the forward part of the leading-edge followed by leading-edge vortex like flow in the aft. Luckring's results [132, 135, 139] show that the attached flow area increases as the angle of the attack decreases (Fig. 30). Also, increasing Reynolds number will expend the attached flow area (Fig. 31). However it is worthwhile to mention that this only happens at a certain range of angle of attack. At a small angle of attack where the attached flow is weak or at high angle of attack where the vortex flow dominates, the Reynolds number effect is small. This can be drawn from comparing Fig. 30 with Fig. 31 at different angles of attack.

Similar to the Reynolds number effect, the free stream turbulence intensity will also affect the experimental results. As the turbulence intensity increases, the unsteadiness in the vortex and vortex breakdown also increase, which will affect the measured results in experiments.

As for the effect of Mach number, Luckring[100-103, 132, 135, 139] has conducted comprehensive experiments on surface pressure. For a sharp leading-edge at small angle of attack, where the vortex flow is weak, the effect of Mach number is minor (Fig. 32). However at high angle of attack, where the vortex flow is stronger, profound Mach number effects can be found in the forward part of the wing (Fig. 33). For a round leading edge, an increase in Mach number will reduce the attached flow area and increase the vortex flow area (Fig. 34). Thus at transonic speed the difference between a round and a sharp leading-edge will become smaller as Mach number increases. The flow will, most likely become leading-edge vortex like flow (compare Fig. 35 with Fig. 11).

2.5 ASSESSMENT FOR THE RESULTS WITH 65º DELTA WING

With those pre-analysis in hand and applying the above mentioned criteria to the results of 65° sweep delta wings, especially for those with large scatter, it was found that:

a). Lambourne & Buyer's[24] experiments were conducted in water tunnel and wind tunnel with a flat upper and bevelled 16º on the lower surface. The ratios of the wingspan to the relevant tunnel span were 61% and 41% resulting in the blockages of 13% and 7.2% for water tunnel and wind tunnel respectively. Moreover the thickness reached $t/c_0=6.3\%$ in the wind tunnel, the highest value among other tests. Although it is not known exactly how much they should be corrected, Weinberg's[35] results

show that the increases of model thickness and blockage could promote vortex breakdown by as much as 20% of centerline chord (i.e., move closer to the wing apex).

b). Earnshaw's[26, 27] results were obtained with a model with t/c_r=4% and symmetrical cubic curve section. According to the equation of the model surface, the section half angle (normal to the leading-edge) at the leading-edge is 14.2°. As the bevel width is comparable with the thickness of the boundary layer before separation, the bevel effect corresponds to a decrease in the effective angle of attack. If the average slope is taken in Earnshaw's experiment, the effective angle of attack could be reduced by as much as 3°.

c). Hanff & Huang's[70-72, 77, 82, 87] early experiments were conducted at the $Re_{c0} \approx 3.6x10^6$ in two different wind tunnels using different model supports. The blockage of the wing model at α=30° is 1.8% and 1.4% for two wind tunnels respectively. The data were repeatable and the differences of the results obtained from two facilities were minor. In the experiments, breakdown location was found by means of a laser sheet normal to the vortex axis and determined by a blurring of the vortex ring. This criterion is consistent with Lambourne's[29] definition for spiral vortex breakdown. Subsequent tests by Huang and Hanff[105] with a laser sheet containing the vortex axis showed the location measured by the criteria to be approximately 10% of centerline chord downstream of the kink point. Moreover, as the experiments were conducted at high Re number resulting in the bevel size relatively larger than the thickness of the boundary layer in the vicinity of the separation area. Thus a 4° angle of attack correction due to leading-edge bevel was proposed by Hanff and Huang [104]. Taking the correction into account, the modified data are close to their later experiments [114] conducted in the water tunnel.

d). Pelletier's[91, 93] experiments were conducted in 2ft by 2ft wind tunnel with the models similar to Hanff & Huang's[104] and Huang's[136] models but half size, c_0=14in, t/c=1.8% and at $Re_{c0} \approx 1\ x10^5$. The blockage is 7.9% at α=30°. Smoke was injected into the free stream near the apex of the model through two small smoke ports. The vortex breakdown was determined by the kink point in the top view. The single-bevel wing has a flat upper surface and bevelled 45º on the lower surface. The double-bevel wing has a symmetric 20º bevel inclusive which is identical to the wing tested by Hanff and Huang [70, 82, 104]. The difference in vortex breakdown locations between the two wing models is less than 5%. The bevel effect on the vortex breakdown location is negligible which agrees with above analysis as the ratio of bevel size to the size of the boundary layer thickness is much smaller than that in the case of Huang and Hanff's experiments.

e). The experiments conducted by Addington and Cipolla's [119, 107] were similar to the model in Huang and Hanff's experiments. In the former, the experiments were conducted in 2ft by 2ft wind tunnel at $Re=2.9x10^5$ while in the later the experiments were conducted in water tunnel at Re=32400. Vortex breakdown was visualized by dye injection from ports on the upper surface near the apex. Their results at α=30º and ϕ=0º falls closer to Huang's[114] water tunnel results.

The original data sets have been assessed and correlated into a delta wing with flat upper surface by the above approach as shown in Fig. 34 which exhibits less scatter and more confidence than in Fig. 4. Further, if we assume a normal probability distribution, the normalized mean value representing time-averaged vortex breakdown location over 65º delta wing with flat upper surface can be obtained as shown in Fig. 35. The R-squared value is 0.96 for the measured results. With 95% interval of confidence based upon the standard deviation (σ) of the results, the true mean for the time-averaged breakdown location is given by

$$x_{vb} = \bar{x}_{vb} \pm t_{v,95}\bar{\sigma}$$

where $\bar{x}_{vb}$ is mean value shown in Fig. 35, $t_{v,95}$ is Student's t value and $\bar{\sigma} = \sigma/\sqrt{N}$.

The largest precision interval is of the order of 4% at $\alpha \approx 30^{o}$.

2.6 ASSESSMENT OF THE RESULTS WITH 70º DELTA WING

In the case of the 70° delta wing, in addition to a scatter similar to that of the 65° wing, a discontinuity movement of the breakdown location in the aft of the wing was observed in Wentz & Kohlman's[33-35] results. Both of them have to be further investigated.

a). Wentz & Kohlmann's[33-35] experiment employed a wing model with non-dimensional thickness (thickness/root chord) $t/c_0 = 0.007$, nearly an order of magnitude less than that in others' experiments. Owning to a 7.5° bevel on the lower surface, the model was further exacerbated on the forward part. Thus the effect of the aeroelastic deformation on vortex behavior has to be considered. The deformation under the reported test conditions in Wentz & Kohlmann's[35] test (q=30 psf) was estimated by the finite element method where the loading was based on the reported breakdown locations, x_{VB}, at the trailing edge, x_{VB}=1, and at x_{VB}=0.4 for $\alpha \approx 29°$ and 30° respectively. The calculated deflections are large and their effects can not be ignored (see Fig. 36 and Fig. 37). Specifically, at $\alpha \approx 30°$ the wing has a negative camber with 1.3° deflection angle at the apex while at $\alpha \approx 29°$ it exhibits a positive camber over most of wing area. In light of the above, it follows that when α decreases from 30°, initially the negative camber will result in a premature vortex breakdown. As α decreases, the vortex breakdown location begins to move downstream. That movement redistributes the load such that it tends to reduce the negative camber which, in turn, makes the breakdown location move further downstream. A positive feedback is clearly present in the coupling between the deformation changes and the loading changes, leading to the reported discontinuous behavior. In fact Wentz & Kohlmann's[35] reported angular deflections, as high as 3~4 degrees at the apex section for these slender delta wings and their possible effect on breakdown location. Considering the above, it is reasonable to assume that discontinuous vortex breakdown location in Wentz & Kohlmann's report for $\Lambda \geq 70°$ delta wing is anomalous due to aeroelastic effects and cannot, therefore, be deemed to be representative of the breakdown behavior over a rigid model. Similar conclusion had been obtained by Lowson[90].

b). Lemay's[56] model has 23° bevel on the upper surface along the leading-edge while Earnshaw's[27] model has a 14° slope on the upper surface. Since the bevel widths are relatively larger than those of Erickson[42],Miau[84] and Huang[114] in their water tunnel experiments, in the Lemay's[56] and Earnshaw's[27] cases the bevel may result in a reduction of the effective angle of attack with corresponding delays in the vortex breakdown location.

c). Mitchell's[128] and Molton's[80] experiments were carefully conducted. However the asymmetric support in the experimental set-up may cause the up wash resulting in the increase of the effective angle of attack, $\Delta\alpha$, and the upstream movement of the vortex breakdown. Actually this up-wash and effective angle of attack increase was observed by earlier experiment conducted by Molton[80] where it was estimated $\Delta\alpha$ could reach 2~3° at high angles of attack range. In addition, the blockage and the flow angularity induced by asymmetric support may cause some problem as the blockage of vertical and horizontal supports was roughly 7% while the model blockage at α=30° was 6.5%. As Lambourne &Bryer's[24] experiments show large blockage which may promote the vortex breakdown.

In viewing of the above considerations, similar to the 65 sweep delta wing the assessed data set and the normalized data set of time-averaged vortex breakdown locations for the 70° delta wing with sharp leading-edges and flat upper surface are depicted in Fig. 38 and Fig. 39 respectively. The largest precision interval is of the order of 5% at $\alpha \approx 40^{\circ}$.

2.7 CONCLUSIONS

- A screening process has been performed on more than eighty experimental cases about vortex breakdown over delta wings with different sweptback angles at high angles of attack and static model conditions. Vortex breakdown locations over 65º and 70º delta wings with flat upper surface have been normalized.
- The effects of leading-edge shape, centerbody and other test conditions have been critically investigated.
- The leading-edge shape may affect the vortex behavior which depends on relative size of the leading-edge shape to the thickness of the boundary layer. Its effect may be neglected if the relative size is small.
- If the relative size is large, different leading edge shapes, e.g. sharp and round leading-edges, may have different effects on the vortex, either at the separation lines or the onset of the separation location. The difference in time-averaged vortex breakdown locations between sharp and round leading-edges needs further clarification.
- For the discussed centerbody setting, no global but only local effect on the pressure has been observed. Centerbody may have minor effect on the vortex breakdown.
- Increase Reynolds number may promote transition in the free shear layer and delay the onset of separation line on round leading-edge. However Reynolds number may have less effect on time-averaged vortex breakdown location, even on wings with round leading edges.
- Increase Mach number results in the reduction of the effect of the leading-edge shape. It also promotes vortex breakdown upstream. Reynolds number Effect

2.8 REFERENCES

[1] Squire, H. B., “Analysis of the Vortex Breakdown Phenomenon,” Part I, Imperial College of Science and Technology, Aeronautics Dept. Report No. 102, 1960.

[2] Hall, M.G., “A Theory for the Core of a Leading-Edge Vortex,” J. Fluid Mech. 11, 209-228, 1961.

[3] Hall, M.G., “The Structure of Concentrated Vortex Cores,” Prog. Aerospace Sci. 7, 53-110, 1966.

[4] Benjamin, T.B., “Theory of the Vortex Breakdown Phenomenon,” J. Fluid Mech. 14(4), 593-629, 1962.

[5] Sarpkaya, T., “On Stationary and Traveling Vortex Breakdowns,” J. Fluid Mech., Vol. 45, Part 3, 1971.

[6] Sarpkaya, T., "Vortex Breakdown in Swirling Conical Flows," AIAA Journal, Vol. 9, Sept. 1971.

[7] Hall, M.G., "Vortex Breakdown," Ann. Rev. Fluid Mech., Vol. 4, 1972..

[8] Leibovich, S., "The Structure of Vortex Breakdown," Ann. Rev. Fluid Mech. 10, 221-246, 1978.

[9] "High Angle of Attack" AGARD CP-247, January 1979.

[10] Wedemeyer, E., "Vortex Breakdown," No. 9, AGARD-LS-121, Dec. 1982.

[11] "Aerodynamics of Vortical Type Flows in Three Dimensions" AGARD-CP 342, July 1983.

[12] Leibovich, S., "Vortex Stability and Breakdown," AGARD-CP-342, No. 23, April 1983.

[13] Leibovich, S., "Vortex Stability and Breakdown: Survey and Extension," AIAA Journal, Vol. 22, No. 9, Sept. 1984.

[14] Leibovich, S., "On a Theoretical Scenario for Vortex Breakdown," Vortex Control and Breakdown Behavior, Second International Colloquium on Vortical Flows, Baden, Switzerland, April 1987.

[15] Delery, J., Pagan, D. and Solignac, J.L., "On the Breakdown of the Vortex Induced by a Delta-Wind," ONERA T.P. nº 1987-105, 1987.

[16] Mario Lee and Ho, C.M., "Lift Force of Delta Wings," Appl Mech Rev, Vol. 43, No. 9, Sept. 1990.

[17] Nelson, R.C. and Visser, K.D., "Breaking Down the Delta Wing Vortex – The Role of Vorticity in the Breakdown Process," AGARD Symposium on Vortex Flow Aerodynamics, October 1-4, 1990.

[18] "Vortex Flow Aerodynamics" AGARD CP-494, July 1991.

[19] Delery, J.M., "Aspect of Vortex Breakdown," Prog. Aerospace Sci. Vol. 30, pp. 1-59, 1994.

[20] "Advanced Flow Management, Part A: Vortex Flow and High Angle of Attack" RTO AVT Symposium May 2001.

[21] Lee, G.H., "Note on the Flow Around Delta Wings with Sharp Leading Edges," ARC R&M 3070, Sept. 1953.

[22] Elle, B.J., "An Investigation at Low Speed of the Flow Near the Apex of Thin Delta Wings with Sharp Leading-Edges," ARC R&M 3176, January 1958.

[23] Elle, B.J., "On the Breakdown at High Incidence of the Leading Edge Vortices on Delta Wings," J. of the Royal Aero. Soc., Vol. 64, August 1960.

[24] Lambourne, N.C. and Bryer, D.W., "The Bursting of Leading-Edge Vortices – Some Observations and Discussion of the Phenomenon," ARC R&M 3282, April 1961.

[25] Harvey, P.M., "Some Observations of the Vortex Breakdown Phenomena," J. Fluid Mech., Vol. 14, 1962.

[26] Earnshaw, P.B. and Lawford, J.A., "Low-Speed Wind-Tunnel Experiments on Series of Sharp-Edged Delta Wings," ARC R&M 3424, March 1964.

[27] Earnshaw, P.B., "Measurements of Vortex-Breakdown Position at Low Speed on a Series of Sharp-Edged Symmetrical Models," ARC CP 828, Nov. 1964.

[28] Lowson, M.V., "Some Experiments with Vorex Breakdown," J. of the Royal Aero. Soc., Vol. 68, May 1964.

[29] Lambourne, N.C., "The Breakdown of Certain Types of Vortex," NPL AERO REPORT 1166, 1965.

[30] Hummel, D., "Research on Vortex Breakdown on Slender Delta Wings," Zeitschrift fur Flugwissenshaften, 13, 5, Aircraft Research Association Ltd., Bedford Library Translation, No. 12, May 1965.

[31] Hummel, D., "Experimental Investigation of the Flow on the Suction Side of a Thin Delta Wing," Z. Flugwiss., Jahrg. 13, Heft 7, pp. 247-252, July 1965

[32] Hummel, D. and Srinivasan, P.S., "Vortex Breakdown on Slender Sharp-Edged Wings," Journal of the Royal Aeronautical Society, Vol. 71, pp.319-322, April 1967.

[33] Earnshaw, P.B., "Measurements of the Effects of Thickness on Vortex Breakdown Position on a Series of Sharp-Edged Delta Wings," ARC CP No. 1018, 1968.

[34] Wentz, W.H. Jr. and Kohlmann, D.L., "Vortex Breakdown on Slender Sharp-Edged Wings" J. Aircraft Vol. 8, No.3, March 1971 or NASA CR 98737, Nov. 1968.

[35] Wentz, W.H. Jr. and Kohlman, D.L., "Wind Tunnel Investigations of Vortex Breakdown on Slender Sharp-Edged Wings," NASA N69-14762, 1968.

[36] Wentz, W.H. Jr., "Wind Tunnel Investigation of Vortex Breakdown on Slender Sharp-Edged Wings," Ph.D. Thesis, University of Kansas, 1969.

[37] Wentz, W.H. Jr., "Effects of Leading-Edge Camber on Low-Speed Characteristics of Slender Delta Wings," NASA-CR-2002, Oct. 1972.

[38] Werle, H., "Sur L'éclatement Des Tourbillons,"ONERA Note Technique, Nº 175, 1971.

[39] Chigier, N.A., "Measurement of Vortex Breakdown over a Delta Wing Using Laser Anemometer," NEAR-TR-62, 1974.

[40] Thompson, D.H., "A Water Tunnel Study of Vortex Breakdown over Wings with Highly Swept Leading Edges," Aerodynamics Note, ARL/A. 356, Australian Defense Scientific Service, May 1975.

[41] Hummel, D., "On the Vortex Formation over a Slender Wing at Large Angles of Incidence," AGARD-CP-247, Oct. 1978.

[42] Erickson, G.E., "Water Tunnel Flow Visualization: Insight Into Complex Three-Dimensional Flow Fields," AIAA Paper 79-1530, also AIAA 80-1423, 1979.

[43] Erickson, G.E., "Vortex Flow Correlation," Tech. Rept. AFWAL-TR-80-3143, 1980.

[44] Erickson, G.E., "Flow Studies of Slender Wing Vortices," AIAA Paper 80-1423, 1980.

[45] Erickson, G.E., "Water-Tunnel Studies of Leading-Edge Voritces," Journal or Aircraft, Vol. 19, No. 6, June 1982.

[46] Skow, A.M. and Erickson, G.E., "Modern Fighter Aircraft Design for High-Angle-of-Attack Maneuvering," AGARD LS121, 4-1 to 4-59, Dec. 1982.

[47] Wedemeyer, E., "Vortex Breakdown," AGARD LS121, 9-1 to 9-17, Dec. 1982.

[48] Escudier, M.P., and Keller, J.J., "Vortex Breakdown: A Two Stage Transition," AGARD-CP-342, No. 25, April 1983.

[49] McKernan, E.C., "An Investigation of the Breakdown of the Leading Edge Voprtices on a Delta Wing at High Angles of Attack," Master Thesis, University of Notre Dame, Jan. 1983.

[50] Gad-el Hak, M. and Blackwelder, R.F., "The Discrete Vortices from a Delta Wing," AIAA Journal, Vol. 23, No. 6, pp. 961-962, June 1985.

[51] Payne, M., Ng, T.T., Nelson, R.C. and Schiff, L., "Visualization and Flow Surveys of the Leading Edge Vortex Structure on Delta Wing Planforms," AIAA Paper 86-0330, 1986.

[52] Boersen, S.J., "US/European Vortex Flow Experriment Test Report of Wind Tunnel Measurements on 65º Delta Wing in the NLR Supersonic Facility SST," NLR TR 86117 U, 1986.

[53] Reynolds, G.A. and Abtahi, A.A., "Instabilities in Leading-Edge Vortex Development," AIAA Paper 87-2424, 1987.

[54] Payne, F. M., "The Structure of Leading Edge Vortex Flows Including Vortex Breakdown," Ph.D. Dissertation, University of Notre Dame, 1987.

[55] Payne, F.M., Ng, T.T., and Nelson, R.C., "Experimental Study of the Velocity Field on a delta Wing," AIAA Paper 87-1231, 1987.

[56] Lemay, S.P., Batill, S.M. and Nelson, R.C., "Leading Edge Vortex Dynamics on a Pitching Delta Wing," AIAA Paper 88-2559, 1988, also J. Aircraft, Vol. 27, No.2 Feb. 1990, pp. 131-138.

[57] McKenan, J.F. and Nelson, R.C., "An Investigation of the Breakdown of the Leading Edge Vortices on a Delta-Wing at High Angles of Attack," AIAA Paper 83-2114. Also J. Aircraft, Vol. 25, No. 11, Nov. 1988.

[58] Lowson, M.V. and Riley, A.J., "The Three Dimensional Vortex Sheet Structure on Delta Wings," AGARD-CP-438, October 1988.

[59] Brandon, J.M. and Shah, G.H., "Effect of Large Amplitude Pitching Motions on the Unsteady Aerodynamic Characteristics of Flat-Plate Wings," AIAA Paper 88-4331, 1988.

[60] Kegelman, J and Roos, F. "Effect of Leading-Edge Shape and Vortex Burst on the Flowfields of a 70 Degree Sweep Delta-Wing," AIAA Paper 89-0086, 1989.

[61] Braslow, A.L. and Collier, F.S., "Applied Aspect of Laminar-Flow Technology," Viscous Drag Reduction in Boundary Layers, Progress in Astronautics and Aeronautics, Vol. 123, 1989.

[62] Panton, R.L., "The Effect of a Contoured Apex on Vortex Breakdown, AIAA Paper 89-0193, 1989.

[63] Magness, C., Robinson, O. and Rockwell, D., "Control of Leading-Edge Vortices on a Delta Wing," AIAA Paper 89-0999, 1989.

[64] Hawk, J.D., Barnett, R.M. and O'Neil, P.J., "Investigation of High Angle of Attack Vortical Flows over Delta Wings," AIAA Paper 90-0101, 1990.

[65] O'Neil, Roos, F.W., Kegelman, R.M., Barnett, R.M. and Hawk, J.D., "Investigation of Flow Characteristics of a Developed Vortex," NADC-89114-60, May 1989, Also AIAA Paper 90-0383, 90-0599.

[66] Roos, F.W. and Kegelman, J.T., "Recent Exploration of Leading-Edge-Vortex Flowfields," McDonnell Douglas Research Laboratories, 1990.

[67] Torlund, P.A., "Force Measurements and Visualization on a 60° Delta Wing in Oscillatory and Stepwise Pitching Motion," ICAS 90-3.3.2, 1990.

[68] Wolffelt, K.W., "Investigation on the Movement of Vortex Burst Position with Dynamically Changing Angle of Attack for a Schematic Delta Wing in a Water Tunnel Correlation to Similar Studies in Wind Tunnel," AGARD CP 413-27.

[69] Roos, F.W. and Kegelman, J.T., "An Experimental Investigation of Sweep Angle Influence on Delta-Wing Flows," AIAA Paper 90-0383, 1990.

[70] Hanff, E.S. and Jenkins, S.B., "Large-Amplitude High Rate Rolling Experiments on a Delta and Double Delta Wing," AIAA Paper 90-0224, 1990.

[71] Hanff, E.S. Kapoor, K., Anstey, C.R. and Prini, A., "Large-Amplitude High-Rate Roll Oscillation System for the Measurement of Non-Linear Loads," AIAA Paper 90-1426, 1990.

[72] Hanff, E.S. and Ericsson, L.E., "Multiple Roll Atractors of a Delta Wing at High Incidence," AGARD CP-494, Oct. 1990.

[73] Gordnier, R.E. and Visbal, M.R., "Numerical Simulation of the Unsteady Vortex Structure over a Delta Wing," AIAA Paper 91-1811, 1991.

[74] Nelson, R.C., "Unsteady Aerodynamics of Slender Wings," AGARD-R-776, pp. 1-1 to 1-26, 1991.

[75] Lowson, M.V., "Visualization Measurements of Vortex Flows," Journal of Aircraft, Vol. 28, No. 5, pp.320-327, May 1991.

[76] Ericsson, L.E., "Analysis of Wind-Tunnel Data Obtained in High-Rate Rolling Experiments with Slender Delta Wings," NRC IAR-CR-14, August 1991.

[77] Hanff, E.S. and Huang, X.Z., "Roll-Induced Cross-Loads on a Delta Wing at HIgh Incidence," AIAA Paper 91-3223, 1991.

[78] Weinberg, X. "Effect of Tunnel Walls on Vortex Breakdown Location over Delta Wings," AIAA Journal Vol. 30, No. 6, June, 1992.

[79] Stahl, W.H., Mahmood, M. and Asghar, A., "Experimental Investigations of the Vorex Flow on Delta Wings at High Incidence," AIAA Journal, Vol. 30, No. 4, pp. 1027-1032, April 1992.

[80] Molton, P., "Etude Experimentale de leclatement tourbillonnaire sur aile delta en coulement incompressible. Caracterisation du champ externe," ONERA Rapport Tech. Nº 5/1147 AN, 1992.

[81] Miller, L.S. and Gile, B.E., "Effects of Blowing on Delta Wing Vortices During Dynamic Pitching," AIAA Paper 92-0407, Also J. Aircraft Vol. 30, No.3, 1993, pp.334-339.

[82] Huang, X.Z. and Hanff, E.S., "Prediction of Leading-Edge Vortex Breakdown on a Delta Wing Oscillating in Roll," AIAA Paper 92-2677, June 1992.

[83] Guglieri, G. and Quagliotti, F.B., "Experimental Investigation of Vortex Dynamics on Delta Wings," AIAA Paper 92-2731, 1992.

[84] Miau, J.J., Chang, R.C. and Chou, J.H., "Nonuniform Motion of Leading-Edge Breakdown on Ramp Pitching Delta Wing," AIAA Journal Vol. 30, No. 7, July 1992.

[85] Visser, K.D. and Nelson, R.C., "Measurements of Circulation and Vorticity in the Leading-Edge Vortex of a Delta Wing," AIAA Journal Vol. 31, No. 1 pp. 104-111, 1993.

[86] Towfighi, J. and Rockwell, D., "Instantaneous Structure of Vortex Breakdown on a Delta Wing via Particle Image Velocimetry," AIAA Journal, Vol. 31, No. 6, pp. 1160-1162, June 1993.

[87] Huang, X.Z. and Hanff, E.S., "Prediction of Normal Force on a Delta Wing Rolling at HIgh Incidence," AIAA Paper 93-3686, 1993.

[88] Rockwell, D., "Three-Dimensional Flow Structure on Delta Wings at High Angle-of-Attack: Experimental Concepts and Issues," AIAA Paper 93-0550, January, 1993.

[89] Straka, W.A. and Hemsch, M.J., "Effect of a Fuselage on the Leading-Edge Vortex Breakdown of a Delta Wing," J. Aircraft, Vol. 31, No. 4, 1994, pp.1002-1005.

[90] Lowson, M.V. and Riley, A.J., "Vortex Breakdown Control by Delta Wing Geometry," AIAA Paper 94-3487, 1994.

[91] Pelletier, A. and Nelson, R.C., "An Experimental Study of Static and Dynamic Vortex Breakdown on Slender Delta Planforms," AIAA Paper 94-1879, 1994.

[92] Gordnier, R.E. and Visbal, M.R., "Unsteady Vortex Structure over a Delta Wing," Journal of Aircraft, Vol. 31 No. 1, pp. 243-248, 1994.

[93] Pelletier, A., "An Experimental Investigation of Vortex Breakdown on Slender Delta Planforms," Final Contract Report, Hessert Center for Aerospace Research, Notre Dame University, August 1994.

[94] Ericsson, L.E., "Comments on Effect of Fuselage on Delta Wing Vortex Breakdown," Journal of Aircraft Vol. 31, No. 4, pp. 1002-1005, 1994.

[95] Gursul, I., Unsteady Flow Phenomena over delta Wings at High Angle of Attack," AIAA Journal, Vol. 32, No. 2, pp. 225-231, Feb. 1994.

[96] Gursul, I. and Yang, H., "On Fluctuations of Vortex Breakdown Location," Physics of Fluids, Vol. 7, No. 1, pp. 229-231, 1995.

[97] Gordnier, R.E. and Visbal, M.R., "Instabilities in the Shear Layer of Delta Wing," AIAA Paper 95-2281, 1995.

[98] Lowson, M.V., Riley, A.J. and Swales, C., "Flow Structure over Delta Wings," AIAA Paper 95-0586, 1995.

[99] Traub, L.W. and Redinioties, O.K., "Instabilities of Vortex Breakdown; Their Structure and Growth," AIAA Paper 95-2308, 1995.

[100] Chu, J. and Luckring, J.M., "Experimental Surface Pressure Data Obtained on Delta Wing Across Reynolds Number and Mach Number Ranges," Vol. 1 – Sharp Leading Edge," NASA TM-4645, February 1996.

[101] Chu, J. and Luckring, J.M., "Experimental Surface Pressure Data Obtained on Delta Wing Across Reynolds Number and Mach Number Ranges," Vol. 2 – Small Leading Edge," NASA TM-4645, February 1996.

[102] Chu, J. and Luckring, J.M., "Experimental Surface Pressure Data Obtained on Delta Wing Across Reynolds Number and Mach Number Ranges," Vol. 3 – Medium Leading Edge," NASA TM-4645, February 1996.

[103] Chu, J. and Luckring, J.M., "Experimental Surface Pressure Data Obtained on Delta Wing Across Reynolds Number and Mach Number Ranges," Vol. 4 – Large Leading Edge," NASA TM-4645, February 1996.

[104] Hanff, E.S. and Huang, X.Z., "Highlights of the IAR/WL High-Alpha Joint Program," NPU/AIAA AFM 96-016, 1996.

[105] Huang, X.Z. and Hanff, E.S., "Unsteady Behavior of Spiral Leading-Edge Vortex Breakdown," NPU/AIAA AFM 96-038, 1996.

[106] Huang, X.Z. and Hanff, E.S., "Surface Flow Topology on a Delta Wing Rolling at High Incidence," NPU/AIAA AFM 96-041, 1996.

[107] Cipolla, K.M., "Structure of the Flow Past a Delta Wing with Variations in Roll Angle," Ph.D. Dissertation, Leigh University, May 1996.

[108] Huang, X.Z., Hanff, E.S. and Jobe, C.E., "Surface Flow Topology on a Delta Wing at High Incidence for a Range of Rol Angles," AIAA Paper 96-2398, 1996.

[109] Ericsson, L.E., "Flow Physics of Critical States for Rolling Delta Wings," Journal of Aircraft Vol. 33, No. 2, pp. 347-352, 1996.

[110] Ericsson, L.E., "Pitch Rate Effects on Delta Wing Vortex Breakdown," Journal of Aircraft Vol. 33, No. 2, pp. 639-642, 1996.

[111] Ericsson, L.E., "Difficulties in Predicting Vortex Breakdown Effects on a Rolling Delta Wing," Journal of Aircraft Vol. 33, No. 3, pp. 477-484, 1996.

[112] Huang, X.Z. and Hanff, E.S., "Unsteady Behavior of Spiral Leading-Edge Vortex Breakdown," AIAA Paper 96-3408, 1996.

[113] Guglieri, G. and Quagliotti, F.B., "Experimental Investigation of Vortex Dynamics on a 65º Delta Wing in Sideslip ," The Aeronautical Journal, March 1997..

[114] Huang, X.Z. Sun, Y.Z., and Hanff, E.S., "Further Investigation of Leading-Edge Vortex Breakdown Over Delta Wings," AIAA Paper 97-2263, 1997.

[115] Huang, X.Z. Sun, Y.Z., and Hanff, E.S., "Circulation Criterion for Leading-Edge Vortex Breakdown over Delta Wings," AIAA Paper 97-2265, 1997.

[116] Ericsson, L.E., "Effect of Angle of Attack on Roll Characteristics of 65 Degree-Delta Wing," Journal of Aircraft Vol. 34, No. 4, pp. 573-575, 1997.

[117] Lowson, M.V. and Riley, A.J., "Development of a Three-Dimensional Free Shear Layer," J. Fluid Mech. 369, pp. 49-89, 1998.

[118] Jobe, C.E., "Vortex Breakdown Location over 65° Delta Wings – Empiricism and Experiment" AIAA Paper 98-2526, 1998.

[119] Addington, G.A., "The Role of Flow Field Structure in Determining the Aerodynamic Response of a Delta Wing," Ph.D. Dissertation, University of Notre Dame, Notre Dame, Indiana, April, 1998.

[120] Ericsson, L.E., "Effect of Fuselage Geometry on Delta Wing Vortex Breakdown," Journal of Aircraft Vol. 35, No. 6, pp. 898-904, 1998.

[121] Huang, X.Z., Lui, T.C. and Hanff, E.S., "Selected Data Set from Static and Rolling Experiments on a 65º Delta Wing at High Incidence," AGARD WG-22, Chapter 16, 1998.

[122] Hummel, D. and Losser, T., "Low Speed Wind Tunnel Experiments on a Delta Wing Oscillating in Pitch," ICAS 98-3.9.3, Sept. 1998.

[123] Ericsson, L.E., "Effect of Fuselage Geometry on Delta Wing Vortex Breakdown," Journal of Aircraft, Vol. 35, No.6, 1998, pp898-904.

[124] Ericsson, L.E., "Vortex Characteristics of Pitching Double-Delta Wings," Journal of Aircraft Vol. 36, No. 2, March-April 1999.

[125] Huang, X.Z. and Hanff, E.S., "Free-to-Roll Trajectory and Related Attractors of a 65 Delta Wing Rolling at High Incidence," AIAA Paper 99-4103, 1999.

[126] Huang, X.Z. and Hanff, E.S., "Visualization of Bifurcating Vortex Breakdown Location Over Slender Delta Wings," 9th International Symposium on Flow Visualization, August 2000.

[127] Ericsson, L.E., "Further Analysis of Fuselage Effects on Delta Wing Aerodynamics, AIAA Paper 2000-0981, 2000.

[128] Mitchell, a. M., Molton, P. Barberis, D. and Délery, J., "Characterization of Vortex Breakdown by Flow Field and Surface Measurements," AIAA Paper 2000-0788, 2000.

[129] Hanff, E.S., Jenkins, J.E., Huang, X.Z., Myatt, J.H., and Addington, G.A., "Highlights of the NRC/USAF/DND Joint Program on Maneuvering Aerodynamics," Canadian Aeronautics and Space Journal, Vol. 47, No. 3, Sept. 2001.

[130] Mitchell, A.M. and Molton, P., "Vortical Substructures in the Shear Layers Forming Leading-Edge Vortices," AIAA Journal, Vol. 40, No. 8, pp. 1689-1692. August 2002.

[131] Ericsson, L.E., "Further Analysis of Fuselage Effects on Delta Wing Aerodynamics," AIAA Paper 2000-0981, 2000.

[132] Luckring, J.M., "Reynolds Number and Leading-Edge Bluntness Effects on 65º Delta Wing Aerodynamics," AIAA Paper 2002-0419, 2002.

[133] Taylor, G.S., Gursul, I., and Greenwell, D.I., "Investigation of Support Interference in High-Angle-of-Attack Testing," Journal of Aircraft Vol. 40, No. 1, pp. 143-152, January-Februray 2003.

[134] Ericsson, L.E., "Multifaced Influence of Fuselage Geometry on Delta-Wing Aerodynamics," Journal of Aircraft, Vol. 40, No.1, pp. 204-206, January-February 2003.

[135] Luckring, J.M., "Transonic Reynolds Number and Leading-Edge Bluntness Effects on a 65º Delta Wing," AIAA Paper 2003-0753, January 2003.

[136] Huang, X.Z., "Comprehensive Experimental Studies on Maneuvering Aerodynamics over Military Wing Configurations in IAR," CASI Paper 357, 2003.

[137] Gordnier, R.E. and Visbal, M.R., "High-Order Compact Difference Schemes Applied to the Simulation of a Low Speed Delta Wing Flow," AIAA Paper 2003-0620, 2003.

[138] Visbal, M.R. and Gordnier, R.E., "On the Structure of the Shear Layer Emanating from a Swept Leading Edge at Angle of Attack," AIAA Paper 2003-4016, 2003.

[139] Luckring, J.M., "Reynolds Number, Compressibility and Leading-Edge Bluntness Effects on 65º Delta Wing Aerodynamics," ICAS 2004-4.1.4, September 2004.

[140] Huang, X.Z., Mebarki, Y. and Benmeddour, A., "Experimental and Numerical Configuration Study on UCAV's Aerodynamics," ICAS 2004-P.7, 2004.

[141] Panton, Ronald L., "Incompressible Flow," A Wiley-Interscience Publication, 1984.

[142] Pirzadeh, S.Z., "Vortical Flow Prediction Using an Adaptive Unstructured Grid Method," RTO AVT Report-084, 2006.

[143] Huang, X.Z., "IAR Program on Maneuvering Aerodynamics over Military Wing Configurations, Vol. II: Surface and Off-Surface Flow Visualization, IAR Report to be published in 2006.

[144] Huang, X.Z., "IAR Program on Maneuvering Aerodynamics over Military Wing Configurations, Vol. III: Aerodynamic Loads at Static and Different Dynamic Motions," IAR Report to be published in 2006.

[145] Huang, X.Z., "IAR Program on Maneuvering Aerodynamics over Military Wing Configurations, Vol. IV: Surface Pressure Measurements at Static and Different Dynamic Motions," IAR Report to be published in 2006.

[146] Klein, C., etc., "Development of PSP Technique for Application on the VFE-2 65º Delta Wing Configuration," AIAA Paper 2006-59, 2006.

[147] Konrath, R., etc., "Analysis of PSP Results Obtained for the VFE-2 65º Delta Wing Configuration at Sub- and Transonic Speeds," AIAA Paper 2006-60, 2006.

[148] Al-Garni, A.Z., etc., "Experimental and Numerical Investigation of 65-deg Delta and 65/40-deg Double-Delta Wings," AIAA Paper 2006-63, 2006.

[149] Benmeddour, A., Mebarki, Y. and Huang, X.Z., "Computational Investigation of the Centerbody Effects on the Aerodynamics of Delta Wings," RTO-AVT Rep. 084, Chapter 20, 2006.

[150] Straka, William A. and Hemsch, Michael J., "Leading-Edge Vortex Breakdown for Wing Planforms with the Same Slenderness Ratio," Journal of Aircraft, Vol. 31, No. 3, 1994.

Table 1 Summary of experimental investigations considered in this Chapter.

Case No.	1	2	3	4
Λ	70	65, (55-70)	45-76	65, 70
Model Type	Half	Full ,Half	Full	Full
L.E.(Upper)	flat	flat	Convex	Convex
L.E.(Lower)	7° bevel	16°	Convex	Convex
T.E.	blunt	blunt		
c	7.75in	8.5in ,47.5in	0.59-1.18ft	18in, 21in
t	.0625in	0.1875, 3in		
t/c (%)	0.8	2.2, 6.32	6	4
Type	water	Water, wind	wind	wind
Test Section Size	5ftx5ft	13inx10in, 9ftx7ft	4ftx3ft	4ft'x3ft
Re_c	0.7x10E6 (12ft/s)	$0.01\sim4.6x10^6$	$0.2\sim0.4x10^6$ (80ft/s)	$1x10^6$
Turbulence				
Support	Semi & false floor	Strut	Sting	Sting
Blockage, *r*	0.25%	13.0% (Half model)	1.70%	5%
Vis. method	Air bubble	Dye, vapor	Fine tufts	Schlieren
Publication	Ref. 22	Ref. 24	Ref. 26	Ref. 27

Case No.	5	6	7	8
Λ	60, 68.2, 76	45-85	60, 65, 70, 75, 80	60-80, 60/70, 70/8(
Model Type	Full	Full	Full	Full
L.E.(Upper)	flat	7.5° bevel		15°
L.E.(Lower)	3°	7.5° bevel		15°
T.E.		7.5° bevel		15°
c	0.625m	10-18"	100-300cm	150mm
t	1.52cm	0.1in		1.8mm
t/c (%)	0.022			
Type	wind	wind	water	water
Test Section Size	1.3 m		0.22mx0.22m	0.25mx0.25m
Re_c	$1.7x10^6$	$0.3\sim1x10^6$	20cm/s	$9.8x10^3$
Turbulence				
Support	Suspended on wires	2-point strut	Sting	Strut
Blockage, *r*	4.60%	1.80%		8.39%
Vis. method	Stethoscope/smoke	Schlieren	Dye	Dye & Bubble
Publication	Ref. 28	Ref. 32-35	Ref. 39	Ref. 40

Case No.	9	10	11	12
Λ	60-80	65	70	70, 75, 80, 85
Model Type	Full	Full	Full	Full
L.E.(Upper)	flat	flat	flat	flat
L.E.(Lower)			26°	25°
T.E.			blunt	
c			16"	16"
t	0.05in		0.75in	0.25"
t/c (%)			4.7	1.56
Type	water	water	wind	wind
Test Section Size	16inx24inx6ft	0.46mx0.6m	2ftx2ft	2ftx2ft
Re_c	$4.1x10^4$	$3x10^4$	$0.225x10^6$	$0.085x10^6$
Turbulence			0.1-0.2%	0.1-0.2%
Support	Sting	Sting	Strut	Strut
Blockage			8%	8%
Vis. method	Dye	Dye	Smoke (section)	Smoke (section)
Publication	Ref. 42-45	Ref. 46	Ref. 49	Ref. 51, 54, 55

Case No.	13	14	15	16
Λ	60	75	70	45, 70, rectangular
Model Type	Full	Full	Full	Full
L.E.(Upper)	flat	flat	23°	flat
L.E.(Lower)	12°	20°	23°	
T.E.	blunt		23°	
c	100mm	0.31m	16.375in	
t	3 mm	4.6mm	0.5in	
t/c (%)	3		3	
Type	water	water	wind	wind
Test Section Size	0.45 x 0.55 m	0.8 x 0.4 m	2inx2in'	12 ft Diameter?
Re_c		0.08m/s~0.2 m/s	$0.26x10^6$	$1x10^5$
Turbulence			0.10%	
Support	Strut	Strut	Strut	Strut
Blockage			8%	
Vis. method	Air bubble		Smoke (Axes)	Smoke
Publication	Ref. 68	Ref. 83	Ref. 56	Ref. 59

Case No.	17	18	19	20
Λ	75	65	60, 70	60
Model Type	Full	Full	Half	Full
L.E.(Upper)	flat	flat	flat	flat
L.E.(Lower)	40°	20º	25°	12°
T.E.			25°	blunt
c	241, 508mm	150mm	76, 54cm	500mm
t	12mm	3.175mm	1.27 cm	4 mm
t/c (%)		2.12	1.7	0.8
Type	water	water	wind	wind
Test Section Size	610x914mm	400x180mm	91cm x74cm	2x2m
Re_c	$1.2\sim3.6x10^4$	25cm/s, $3.5x10^4$	$0.3\sim2x10^6$	$0.7\sim1.43x10^6$
Turbulence			0.20%	0.1~0.2%
Support	Sting	Strut	Semi & splitter	Strut
blockage			7.80%	
Vis. method	Dye, Hydrogen bubble	Fluorescent dye	Smoke (section)	Smoke/Schlieren
Publication	Ref. 63	Ref. 62	Ref. 65	Ref. 67

Case No.	21	22	23	24
Λ	65	59, 63.4, 67, 70	60, 76	75
Model Type	Full	Full	Full	Full
L.E.(Upper)	flat	blunt	5.7, 11.3	flat
L.E.(Lower)	30		5.7, 11.3	25
T.E.	30	blunt	blunt	
c	850mm	15, 19, 20 cm	0.27, 0.31m	16in
t	20mm	1mm	1.27mm	0.25in
t/c (%)	2.35			1.56
Type	wind	water	water	wind
Test Section Size	3 m (Diameter)	60x60 cm	0.61 x 0.91 m	2inx2in
Re_c	$5.8\sim2.1x10^6$	$9x10^3$	$3.3x10^4$ (0.12m/s)	$0.25x10^6$
Turbulence	0.30%	0.80%		
Support	Sting	Sting	Sting	Strut
blockage		2.10%		6.00%
Vis. method	Helium-soap bubble	Dye	Dye	Anemometer
Publication	Ref. 83	Ref. 84	Ref. 81	Ref. 81

Case No.	25	26	27	28
Λ	65	66.33, 69.33 (W+B)	50 to 80, in steps of 5	65, 70, 75, 80, 85
Model Type	Full	Full	Full	Full
L.E.(Upper)	12	blunt	flat/10	
L.E.(Lower)	12	blunt	45/10	
T.E.	12	blunt	blunt/10	
c	2.04ft	9.483in	8in, 14in	
t	0.375in	0.05in	0.25in	
t/c (%)	1.53	0.5		
Type	wind	water	wind	wind
Test Section Size	7ftx10ft	16inx24in	2ftx2ft	0.8mx0.6m
Re_c	3.6x10E6	0.25ft/s $1.85x10^4$	$0.05\text{-}0.1x10^6$	
Turbulence			0.1-0.2%	0.05%
Support	Sting	Sting	Sting	
Blockage			7.93%	
Vis. method	Smoker/Laser	Dye	Smoke (top)	
Publication	Ref. 70, 71, 72, 87	Ref. 150	Ref. 91, 93	Ref. 90

Case No.	29	30	31	32
Λ	65 (W+B)	65	55, 60, 65, 69, 70, 71, 75	55, 65
Model Type	Full	Full	Full	Full
L.E.(Upper)	10	sharp/round	flat/bevel	flat/bevel
L.E.(Lower)	10	sharp/round	bevel/flat	flat/bevel
T.E.	10			
c	202 mm	25.734in	5in	18-24in
t		0.875in	0.08in	0.375in
t/c (%)				
Type	wind	wind	water	wind
Test Section Size	1m	8.2x8.2ft	15"x20"	6ftx9ft
Re_c		$6x10^6\text{-}120x10^6$	36000/ft	$2x10^6\text{-}3.6x10^6$
Turbulence				
Support		Sting	Sting	Sting
Blockage	3.62%			
Vis. method		pressure taps	Dye	PSP, pressure taps
Publication	Ref. 107	Ref. 100-103, 132,	Ref. 114	Ref. 140

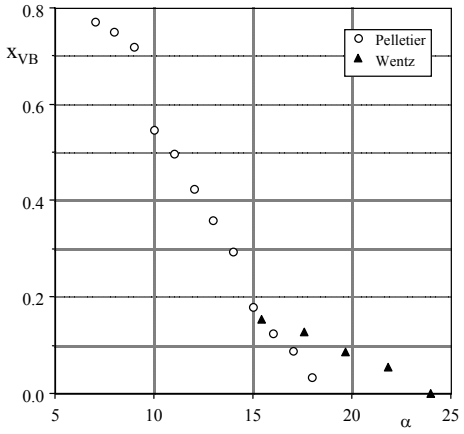

Fig. 1 Vortex breakdown location on 50° delta wing

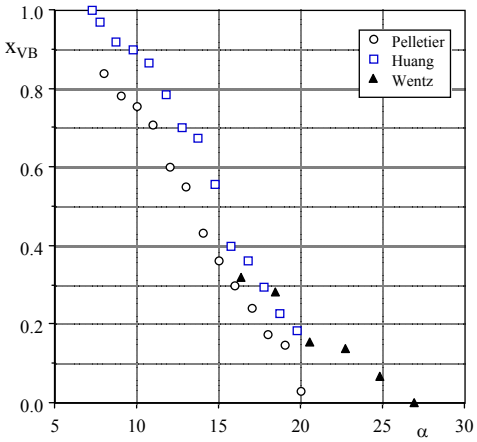

Fig. 2 Vortex breakdown location on 55° delta wing

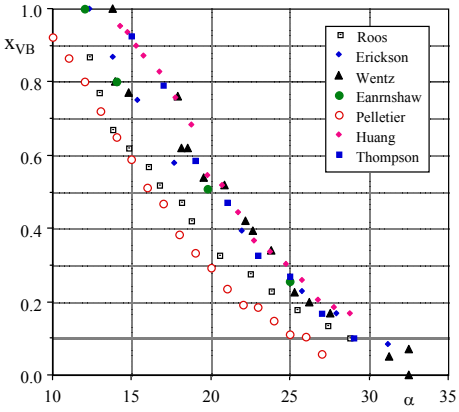

Fig. 3 Vortex breakdown location on 60° delta wing

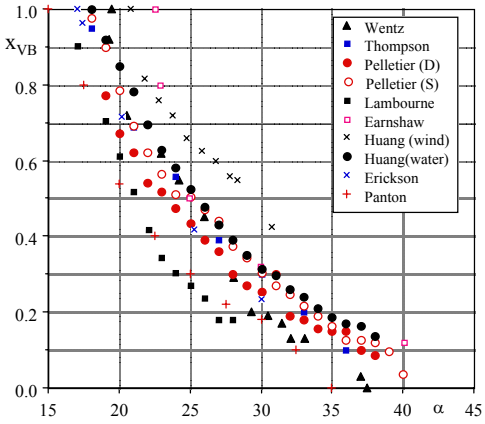

Fig. 4 Vortex breakdown location on 65° delta wing

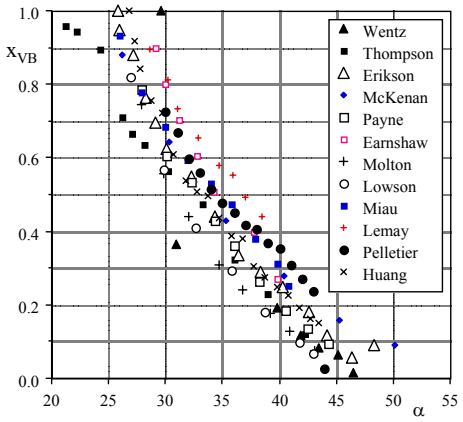

Fig. 5 Vortex breakdown location on 70° delta wing

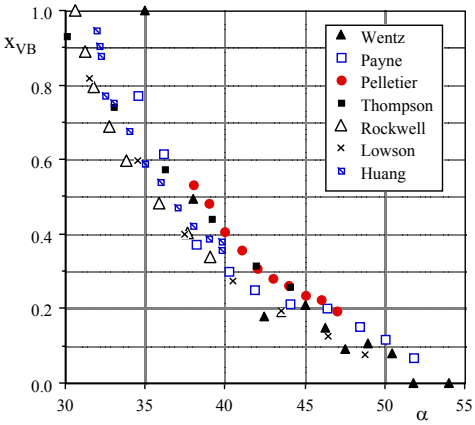

Fig. 6 Vortex breakdown location on 75° delta wing

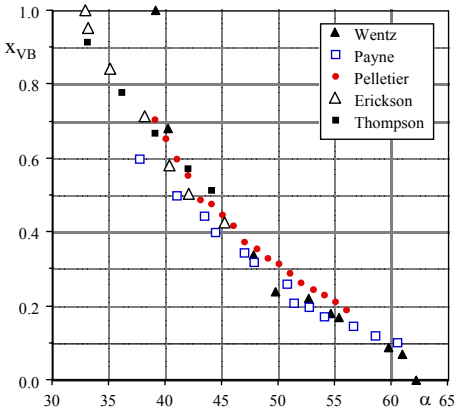

Fig. 7 Vortex breakdown location on 80° delta wing

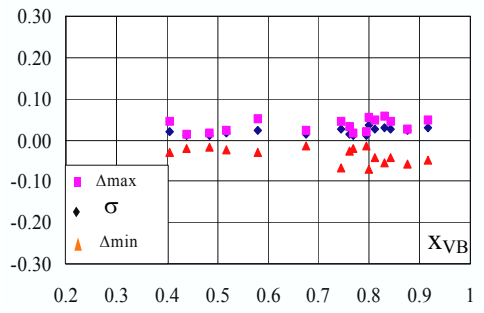

Fig. 8 Standard and maximum deviations of measured vortex breakdown location

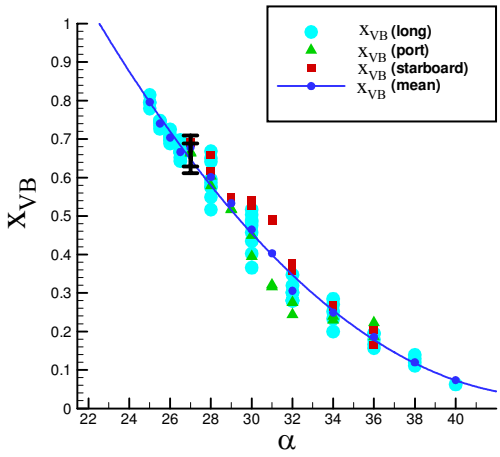

Fig. 9a Deviation in measured breakdown location

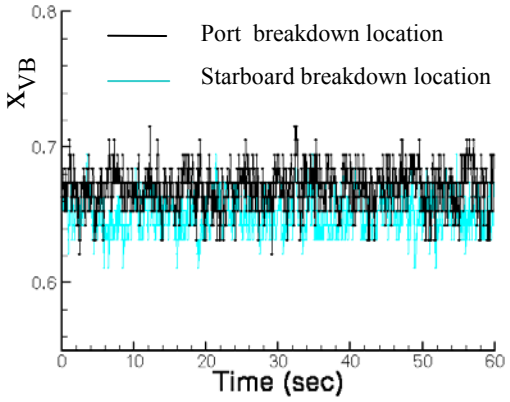

Fig. 9b Time histories of the port and starboard breakdown locations

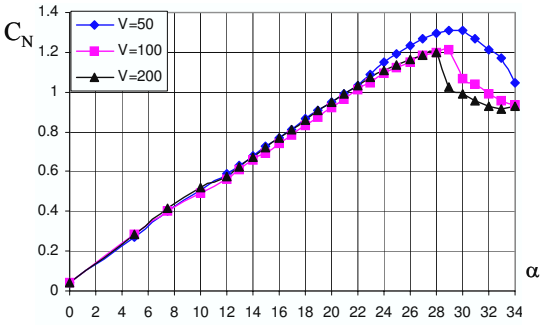

Fig. 10a Measured normal force (flat upper)

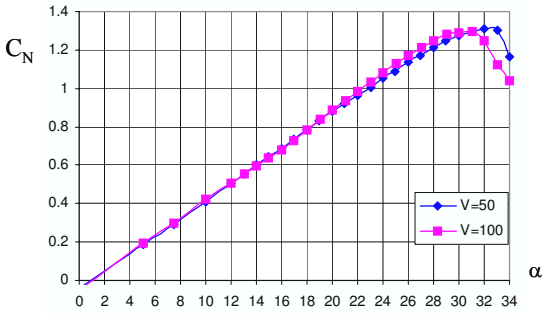

Fig. 10b Measured normal force (bevel upper)

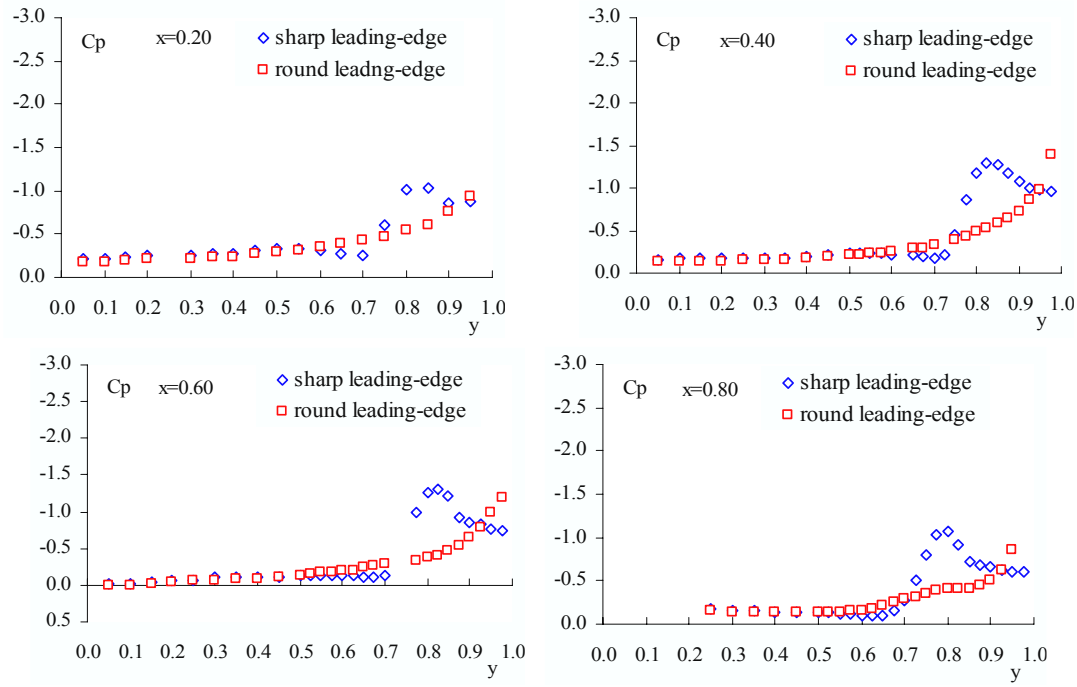

Fig. 11 Comparisons of surface pressure between sharp and round leading edges, M=0.4, Re=6x10^6, α=10º

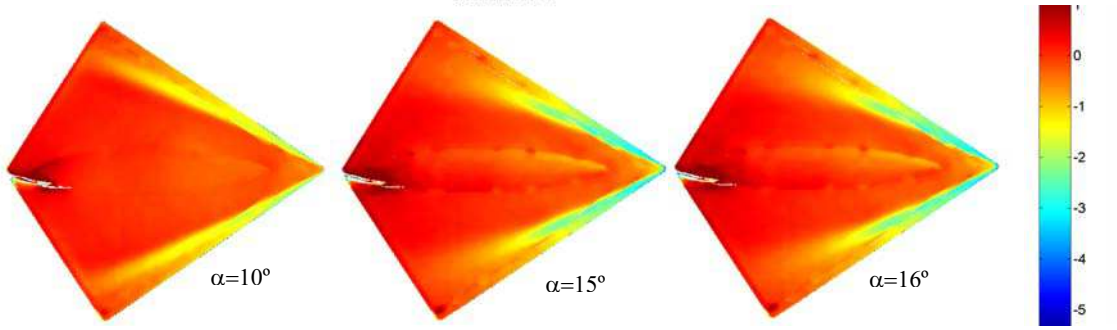

Fig. 12a PSP images on sharp leading-edge at different angles of attack

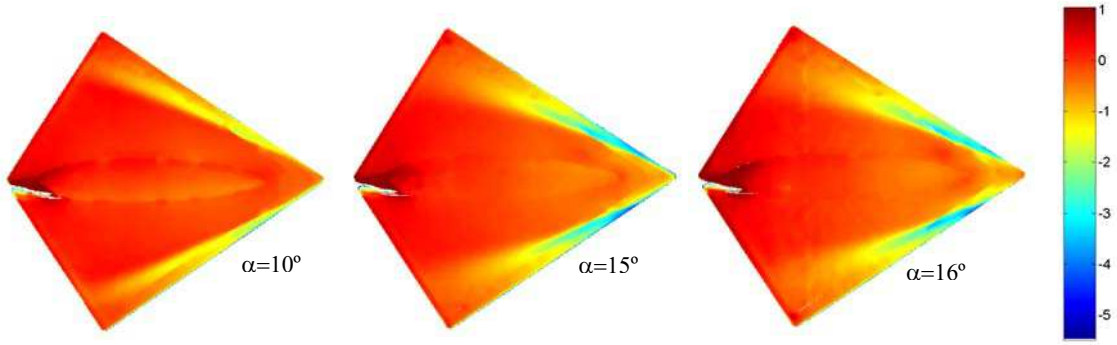

Fig. 12b PSP images on round leading-edge at different angles of attack

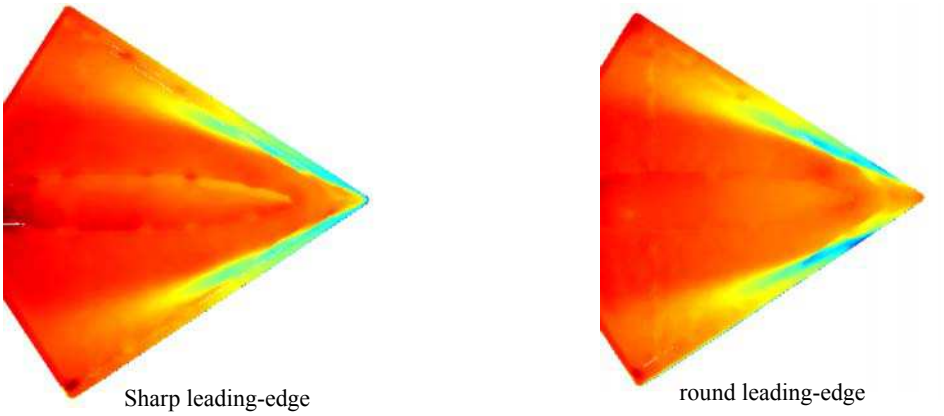

Sharp leading-edge round leading-edge

Fig. 12c enlarged PSP images on sharp and round leading-edge wing models (α=16º)

Fig. 12 PSP measurements at different model conditions

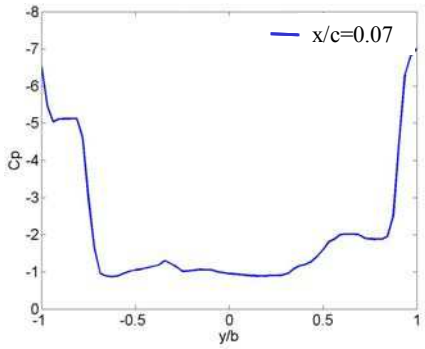

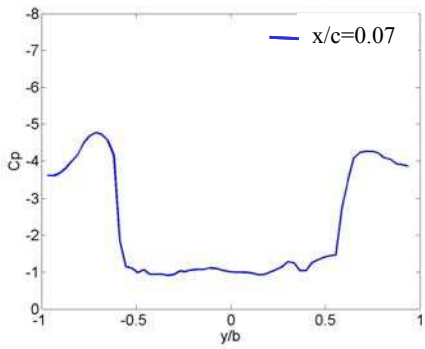

Fig. 13a round leading-edge Fig. 13b Sharp leading-edge

Fig. 13 Digitized PSP results on leading-edge shape effect (U=60 m/s, α=21°)

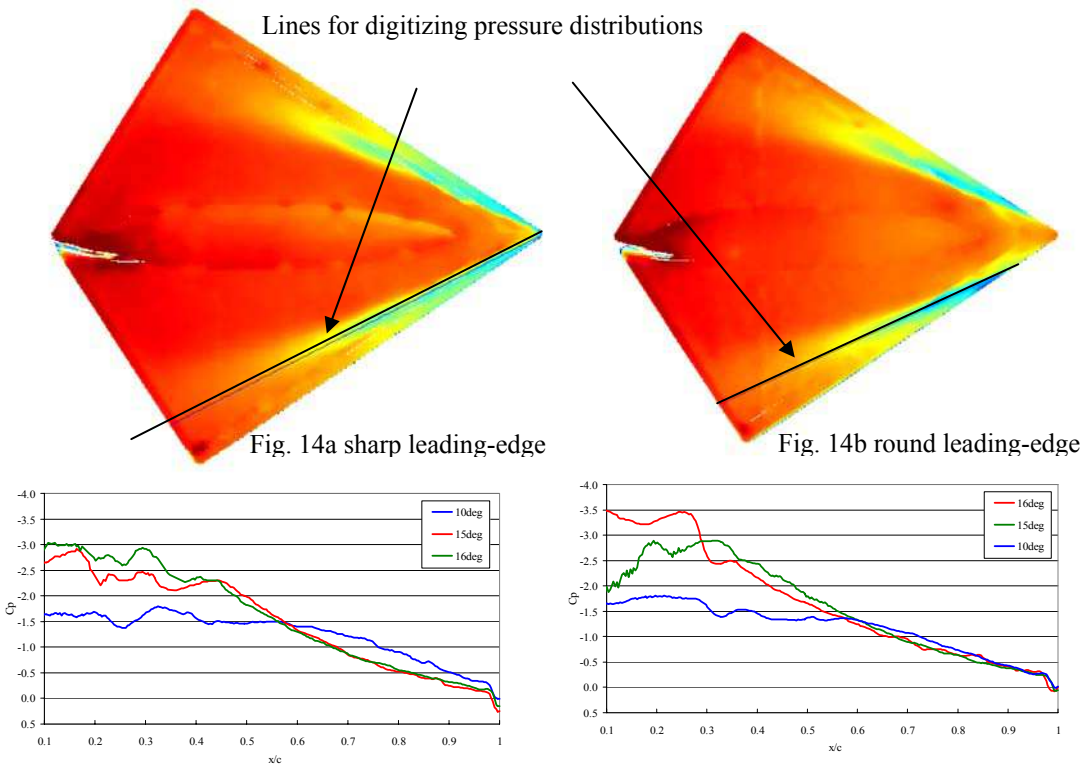

Fig. 14a sharp leading-edge

Fig. 14b round leading-edge

Fig. 14 Digitized pressure distributions on wings with sharp and round leading-edges

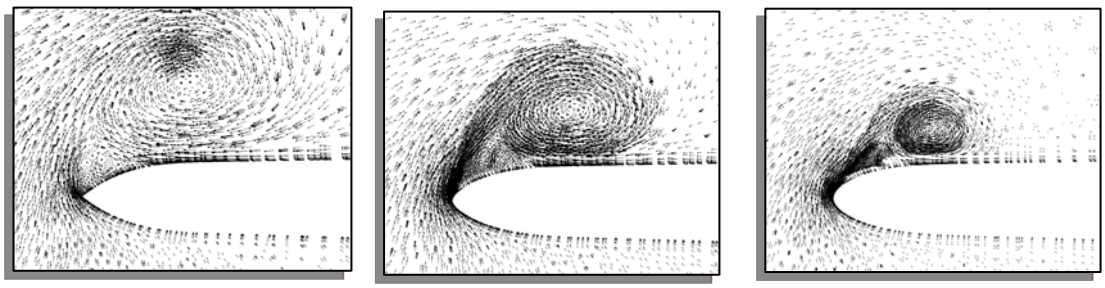

Fig.15a

Fig.15b

Fig. 15c

Fig. 15: Delta wing velocity vectors on cross-sectional planes at the mid-root chord stations showing primary, secondary, and "tertiary" vortices: (a) sharp leading edge, (b) medium leading edge, and (c) large leading edge. Navier-Stokes solutions at M_∞=0.4, α=20°, and Re_{MAC}=6.0x10^6.

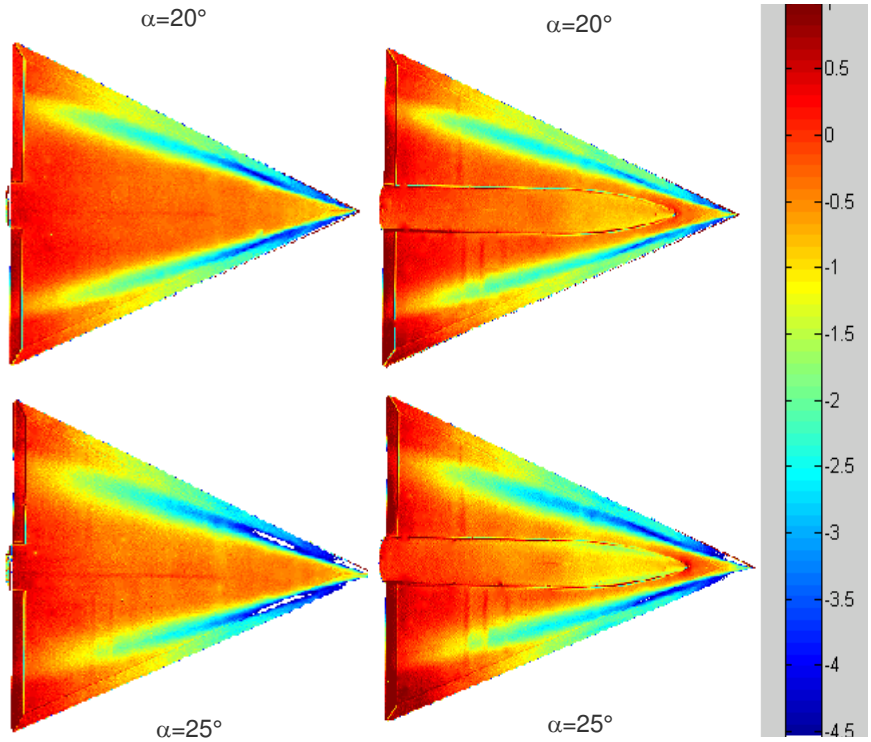

Fig. 16 PSP images between with/without centerbody

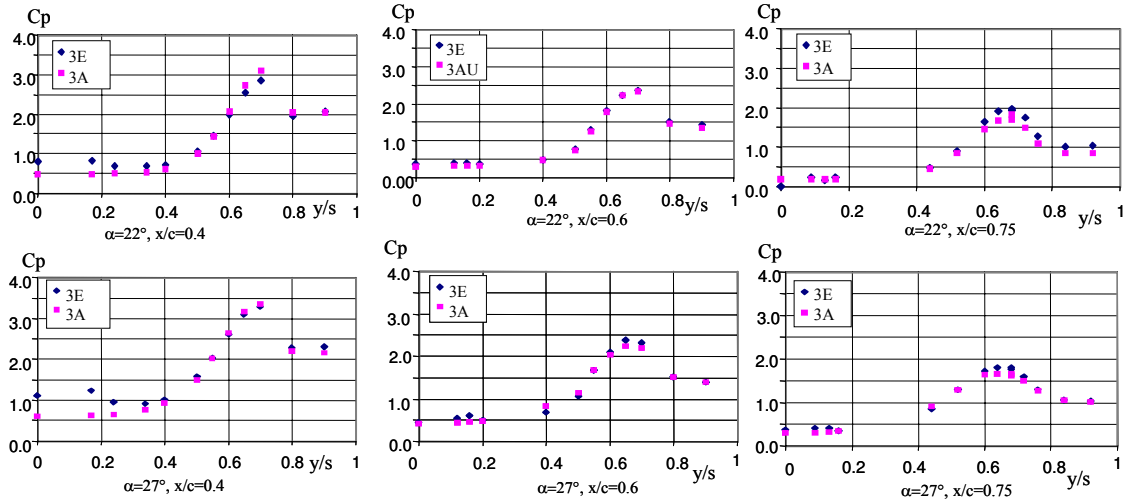

Fig. 17 Centerbody effect on pressure distributions at different locations, U=60m/s
(3E with centerbody; 3A without centerbody)

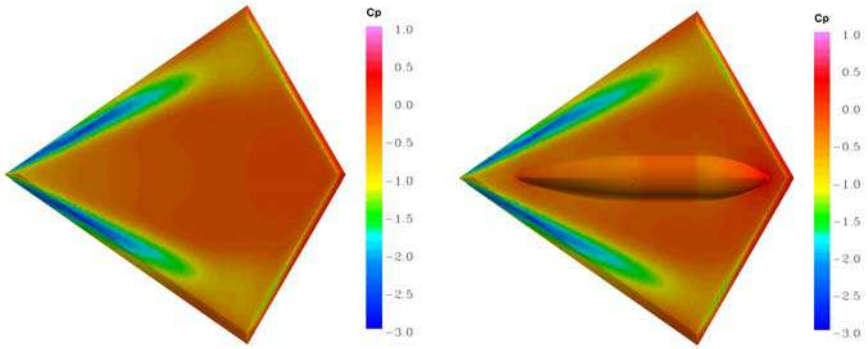

Fig. 18 Comparison of surface pressure between with and without centerbody (Model G1, M=0.18, α=15°)

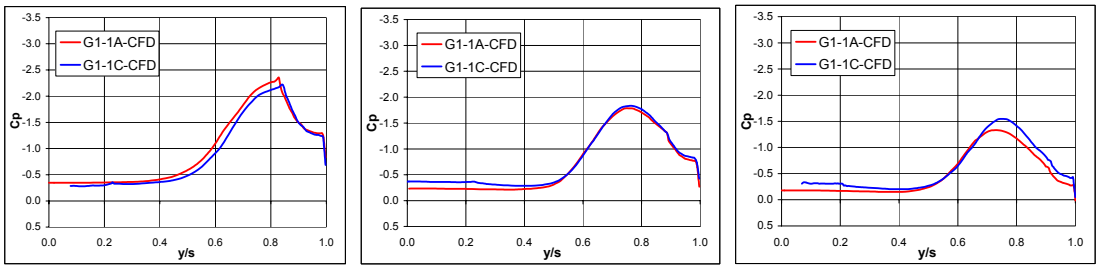

Fig. 19 Comparisons of pressure distributions between with/without centerbody at different chordwise locations (M=0.18, α=15, NF no centerbody, 3E with centerbody)

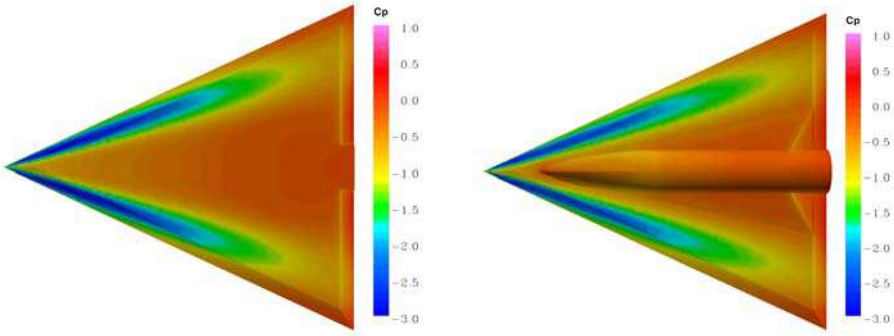

Fig. 20 Comparison of surface pressure between with and without centerbody (Model G2, M=0.17, α=21°)

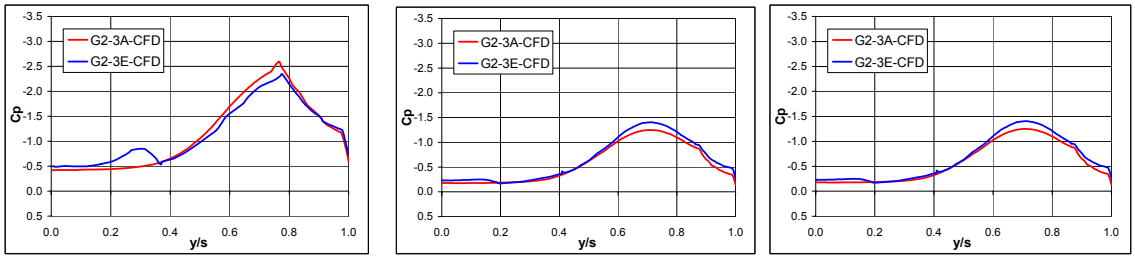

Fig. 21 Comparisons of pressure distributions between with/without centerbody at different chordwise locations (M=0.17, α=21°, 3A no centerbody, 3E with centerbody)

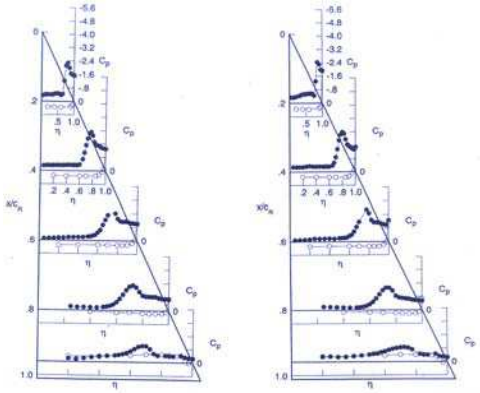

Re=5.8x10^6, M=0.4 Re=60x10^6, M=0.4

Fig. 22 Re number effect on surface pressure with sharp leading-edge

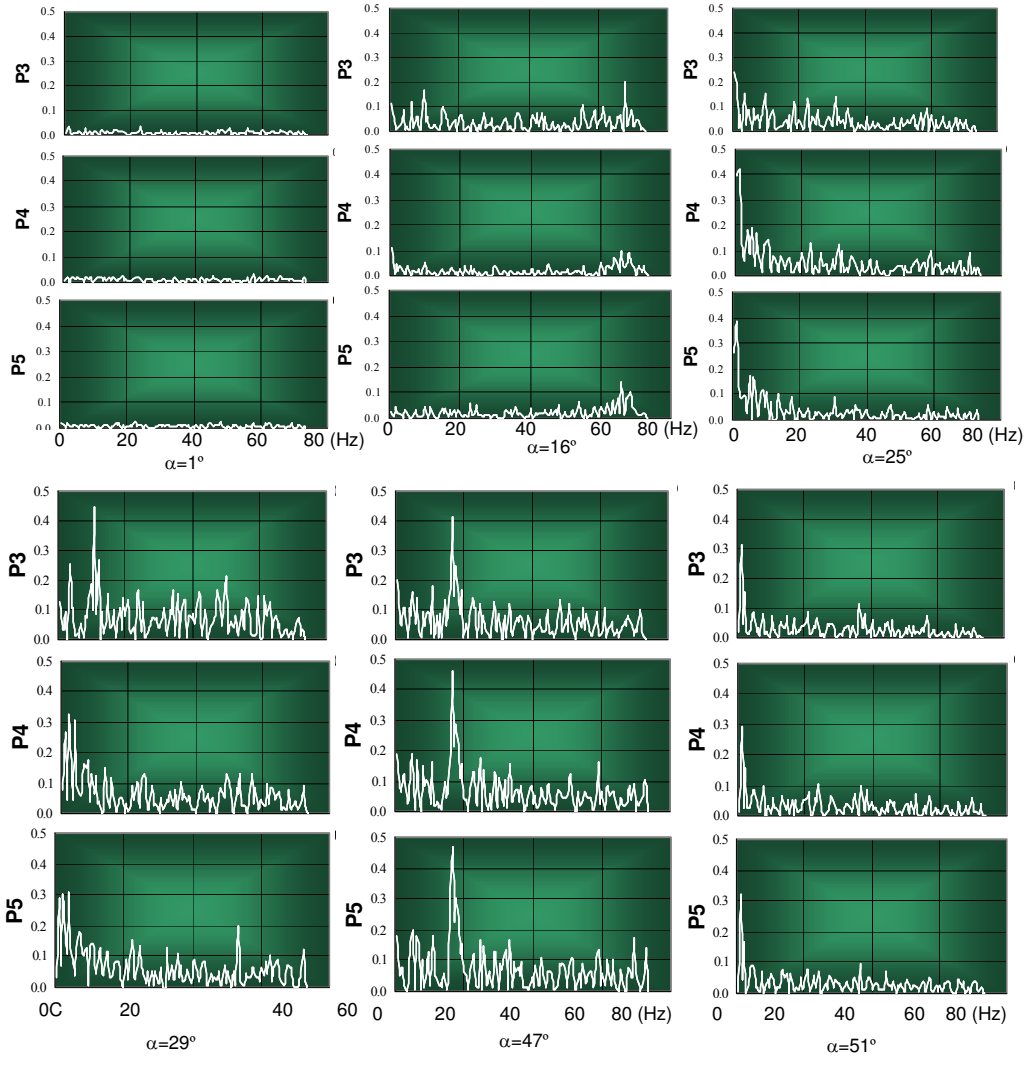

Fig. 23 Unsteady pressure spectral on 65º delta wing at different static angles of attack

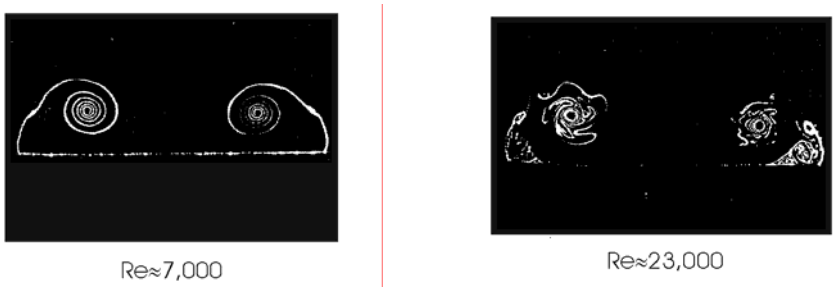

Fig. 24: Flow visualization of shear layer over delta wing

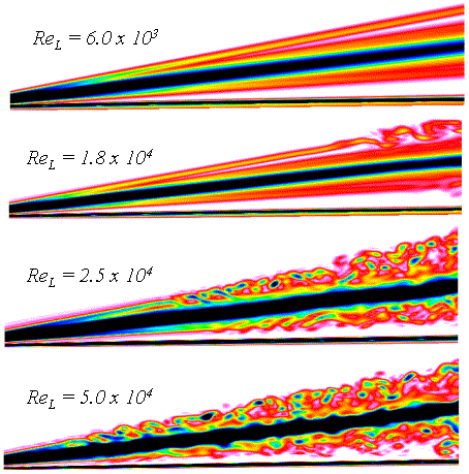

Fig. 25. Evolution of vortex structure with increasing Reynolds number. Contours of instantaneous vorticity magnitude on vertical plane through vortex core

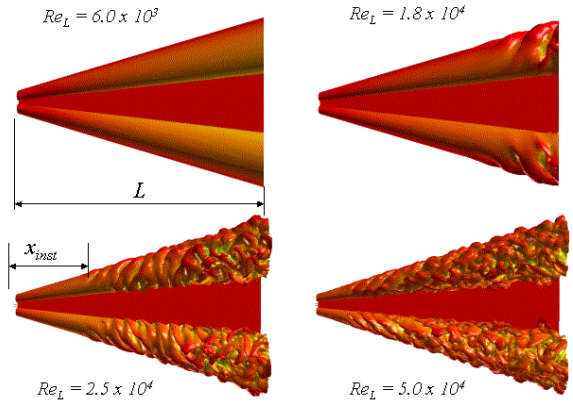

Fig. 26. Evolution of shear layer structure with increasing Reynolds number depicted using an isosurface of axial vorticity

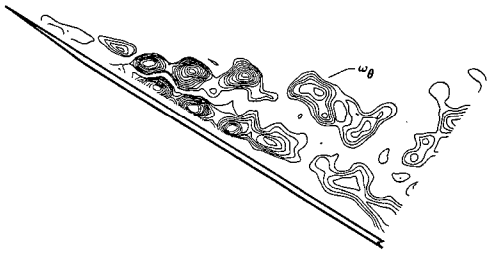

Fig. 27: Instantaneous azimuthal vorticity distribution in a plane that passes through the axis

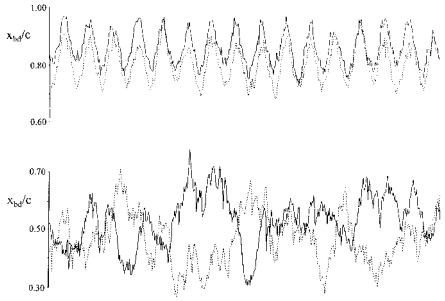

Fig. 28: Time histories of breakdown locations for left and right breakdowns for α_0=29° (top) and α_0=42° (bottom)

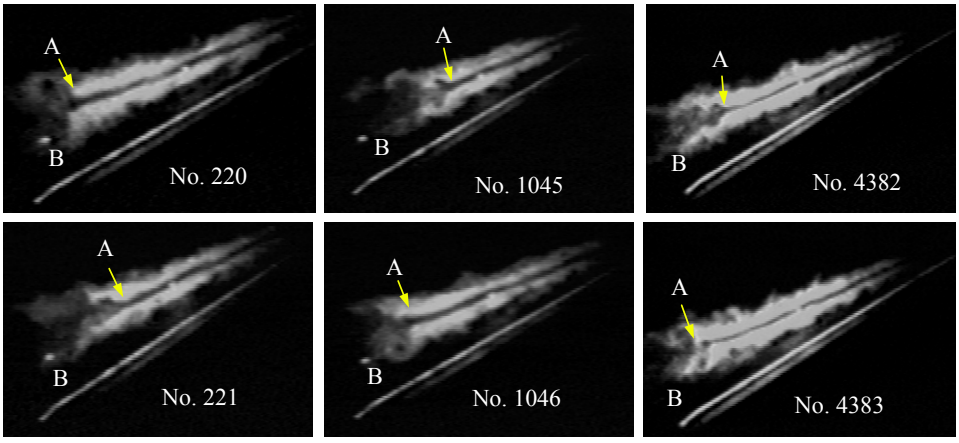

Fig. 29 Sequence of frames of laser-light sheet images

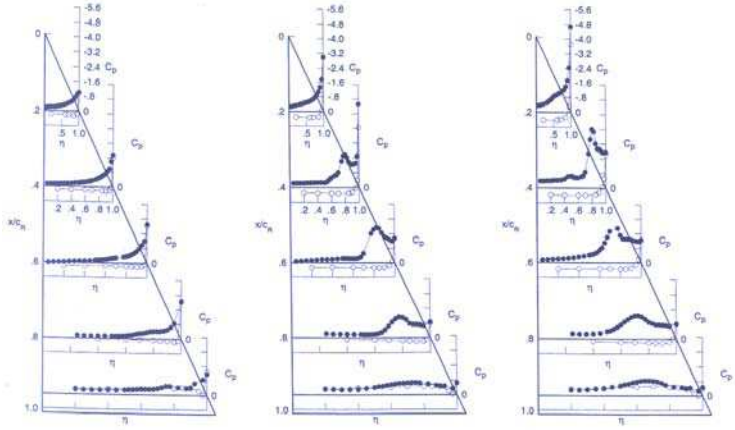

Fig. 30a α=10.3º Fig. 30b α=16.4º Fig. 30c α=20.2º

Fig. 30 Effect of angle of attack on surface pressure of round leading edge, M=0.4, Re=6x10^6

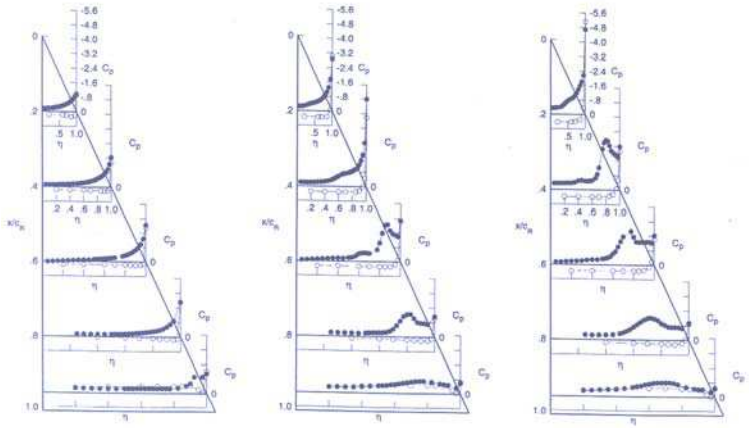

Fig. 31a α=9.9º Fig. 31b α=16.1º Fig. 31c α=20.2º

Fig. 31 Effect of Re number increase on surface pressure of round leading edge, M=0.4, Re=60x10^6

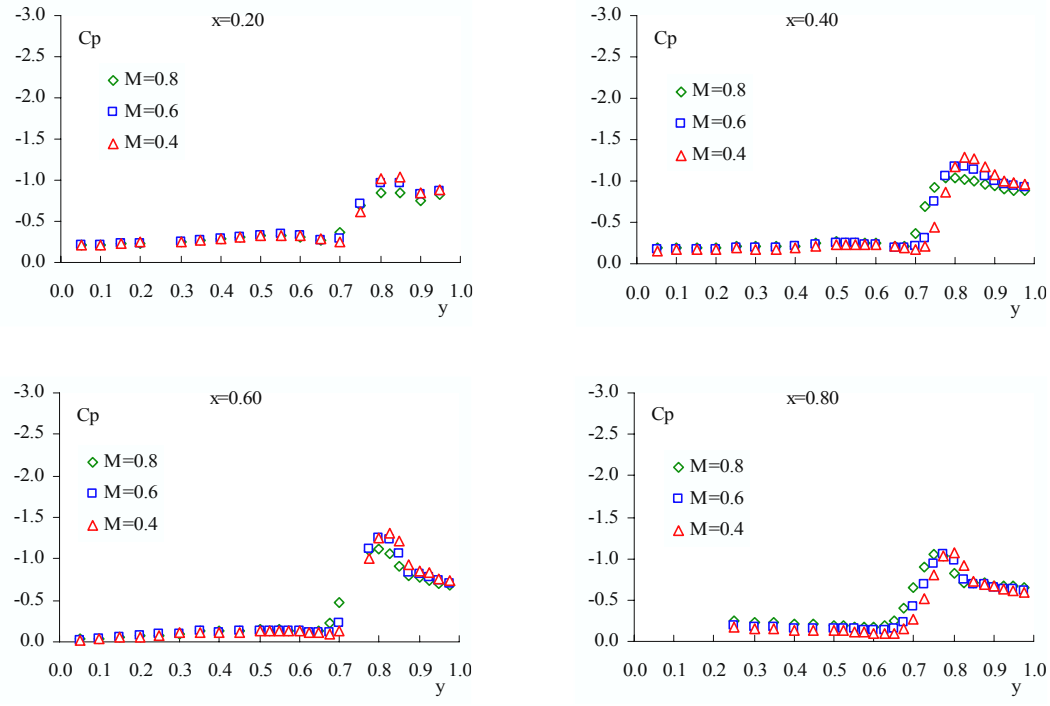

Fig. 32 Mach number effect on surface pressure with sharp leading-edge, Re=6x10^6, α=10º

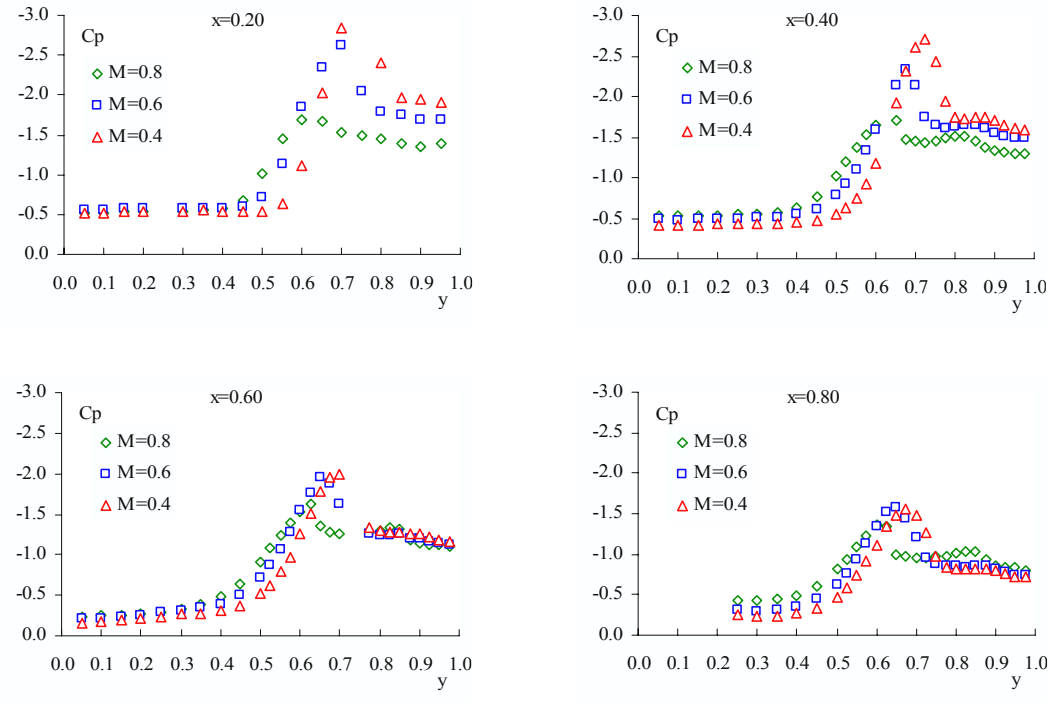

Fig. 33 Mach number effect on surface pressure with sharp leading-edge, Re=6x10^6, α=20º

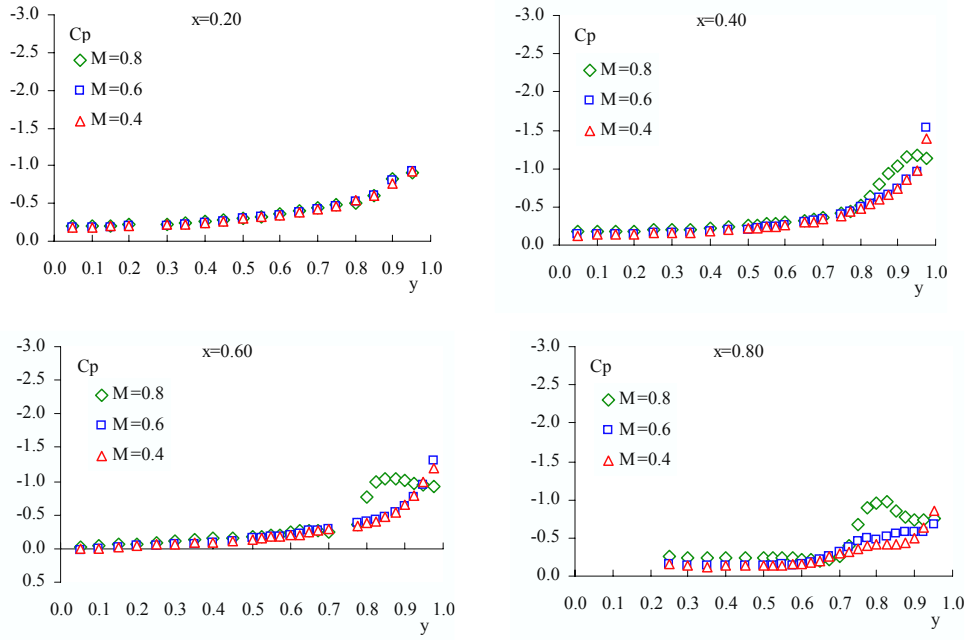

Fig. 34 Mach number effect on surface pressure with round leading-edge, Re=6x10^6, α=10º

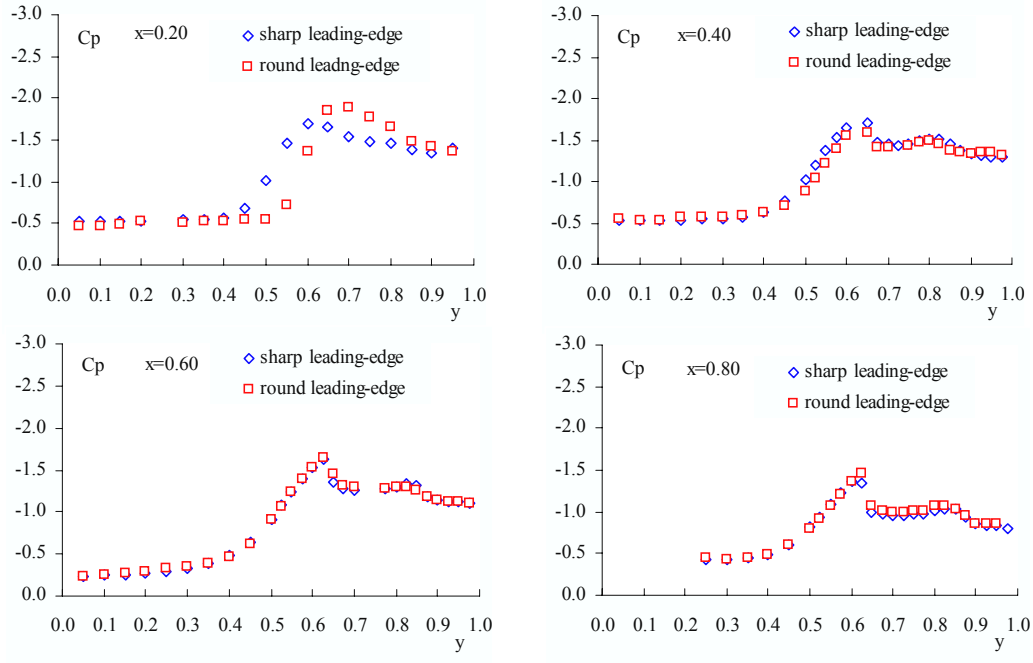

Fig. 35 Comparisons of Mach number effects between sharp and round leading-edge, M=0.8, Re=6x10^6, α=20º

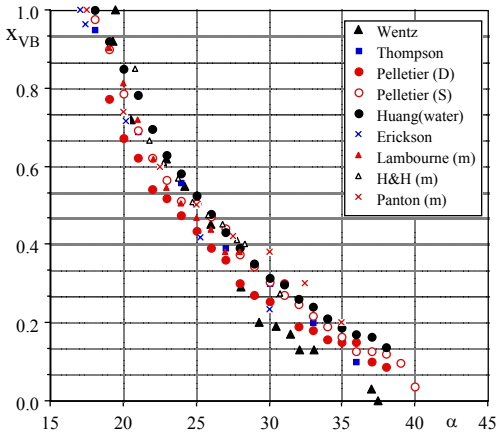

Fig. 36 Assessed results for 65° delta wings

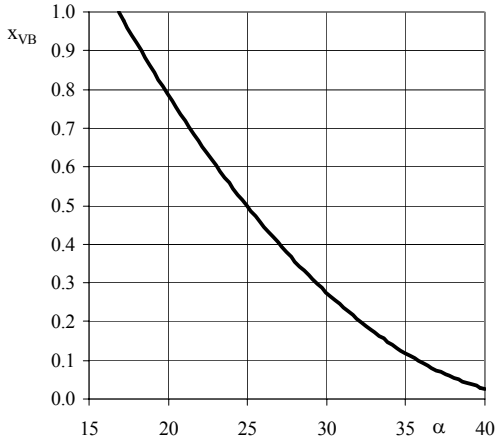

Fig. 37 Normalized results for 65° delta wings

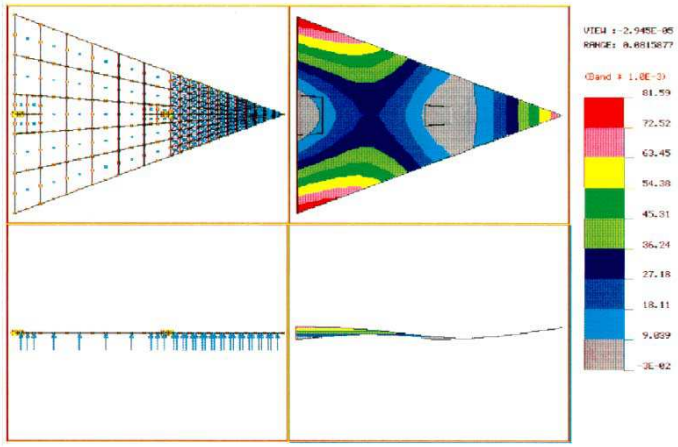

Fig. 38 Deformations estimated at α=30° and x_{VB}=0

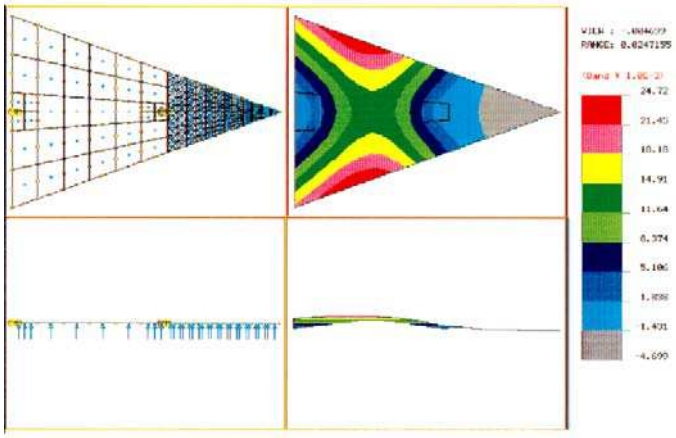

Fig. 39 Deformations estimated at α=29° and x_{VB}=1

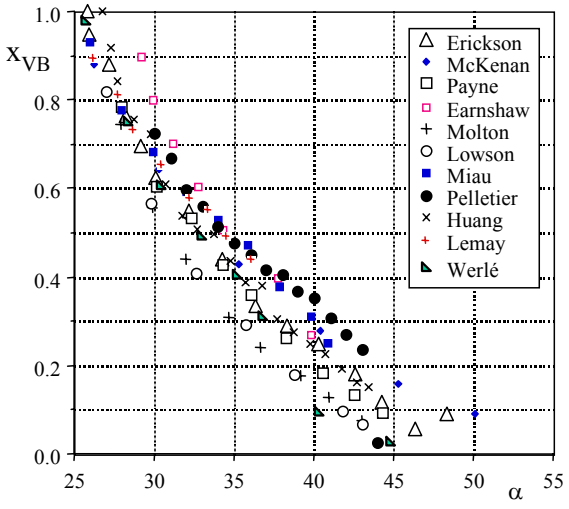

Fig. 40 Assessed results for 70° delta wings

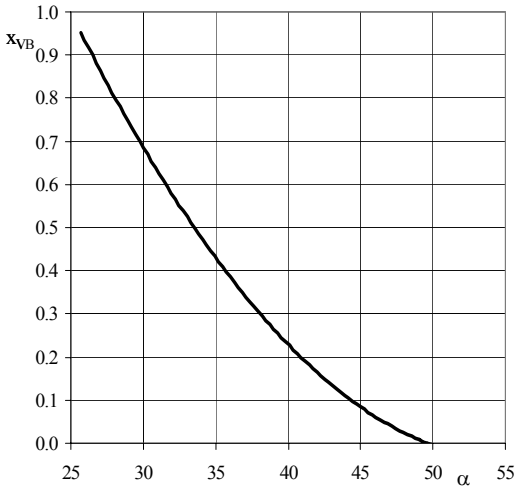

Fig. 41 Normalized results for 70° delta wings